Thermodynamic Analysis of a Multi-Generation Plant Driven by Pine Sawdust as Primary Fuel

Behzad Panahirad

Submitted to the
Institute of Graduate Studies and Research
in partial fulfillment of the requirements for the degree of

Master of Science
in
Mechanical Engineering

Eastern Mediterranean University
February 2017
Gazimağusa, North Cyprus

Approval of the Institute of Graduate Studies and Research

Prof. Dr. Mustafa Tümer
Director

I certify that this thesis satisfies the requirements as a thesis for the degree of Master of Science in Mechanical Engineering.

Assoc. Prof. Dr. Hasan Hacışevki
Chair, Department of Mechanical Engineering

We certify that we have read this thesis and that in our opinion it is fully adequate in scope and quality as a thesis for the degree of Master of Science in Mechanical Engineering.

Prof. Dr. Uğur Atikol
Supervisor

Examining Committee

1. Prof. Dr. Uğur Atikol

2. Prof. Dr. Fuat Egelioğlu

3. Asst. Prof. Dr. Murat Özdenefe

ABSTRACT

The current study is based on a combined heat and power system with multi-objectives, driven by biomass. The system consists of a combustion chamber (CC), a single effect absorption cooling system (SEACS), an air conditioning unit (AC), a reheat steam Rankine cycle (RSRC), an organic Rankine cycle (ORC) and an electrolyzer. The purpose of this system is to produce hydrogen, electricity, heat, cooling, and air conditioning. All the simulations had been performed by Engineering Equation Solver (EES) software. Pine sawdust is the selected biofuel for the combustion process. The overall utilization factor (ε_{en}) and exergetic efficiency (ψ_{ex}) were calculated to be 2.096 and 24.03% respectively. The performed renewable and environmental impact analysis indicated a sustainability index of 1.316 (SI), and a specific CO_2 emission of 353.8 kg/MWh. The parametric study is conducted based on the variation of ambient (sink) temperature, biofuel mass flow rate, and boilers outlet temperatures. The parametric simulation showed that the increase in biofuel mass flow rate has a positive effect on the sustainability of the system. It is noticed that by increasing the biofuel mass flow rate from 0.123 kg/s to 0.22 kg/s, the sustainability index rises from 1.309 to 1.542. However, any increase in boilers outlet temperature and sink temperature, result in a decrease of sustainability index.

Keywords: biomass, exergy assessment, multi-objective plant, CO_2 emission, irreversibility.

ÖZ

Mevcut çalışma biyokütle ile tahrik edilen, çok amaçlı bir bileşik ısı ve güç sistemi üzerine yapılmıştır. Sistem, bir yanma odası (CC), bir tek etkili absorpsiyonlu soğutma sistemi (SEACS), bir hava şartlandırma sistemi (AC), bir tekrar ısıtmalı buhar Rankine çevrimi (RSRC), bir organik Rankine çevrimi (ORC) ve bir elektrolizörden oluşmaktadır. Bu sistemin amacı hidrojen, elektrik, ısı, soğutma üretmek ve hava şartlandırmaktır. Bütün simulasyonlar, Mühendislik Denklem Çözücü (EES) yazılımı ile yapılmıştır. Yanma işleminde kullanılmak üzere seçilen biyokütle, çam talaşıdır. Toplam yararlanma faktörü (ε_{en}) ve ekserji verimliliği (ψ_{ex}) sırasıyla %2.096 ve 24.03 olarak hesaplanmıştır. Gerçekleştirilen yenilenebilir ve çevresel etki değerlendirmeleri sonucunda, sürdürülebilirlik endeksi 1.316 (SI) ve özgül karbondiyoksit salınımı 353.8 kg/MWh bulunmuştur. Yapılan parametrik çalışma çevre sıcaklığını, biyoyakıt kütle akış hızı ve kazanların çıkış sıcaklıkları baz alınarak yapılmıştır. Parametrik simulasyon sonucu, biyoyakıt kütle akış hızı arttırıldığı zaman sürdürülebilirlik endeksinin olumlu etkilediği gözlemlenmiştir. Görülmüştür ki biyoyakıt kütle akış hızı 0.123 kg/s den 0.22 kg/s ye artırıldığı zaman sürdürülebilirlik endeksi 1.309'dan 1.542'ye çıkıyor. Ancak kazan çıkış sıcaklığı veya çevre sıcaklığı artırıldığı zaman sürdürülenilirlik endeksinin düştüğü gözlemlenmiştir.

Anahtar kelimeler: biyokütle, ekserji değerlendirmesi, çok-amaçlı santral, karbondiyoksit salınımı, geri çevrilmezlik.

To My Family

ACKNOWLEDGMENT

I would like to record my gratitude to Prof. Dr. Uğur Atikol for his supervision, advice, and guidance from the very early stage of this thesis as well as giving me extraordinary experiences throughout the work. Above all and the most needed, he provided me constant encouragement and support in various ways. His ideas, experiences, and passions have truly inspired and enriched my growth as a student. I am indebted to him more than he knows.

I would like to thank my family members specially my parents for all their supports throughout my life.

TABLE OF CONTANTS

LIST OF FIGURES

LIST OF TABLES

LIST OF SYMBOLS

$\dot{m}$	Mass Flow Rate (kg/s)
v	Specific Volume (m^3/kg)
p	Pressure (kPa)
h	Enthalpy (kJ/kg)
T	Temperature (°C, K)
W	Work (kW)
$\dot{Q}$	Heat Flow Rate (kW)
HHV	High Heating Value (kJ/kg)
LHV	Low Heating Value (kJ/kg)
Ex	Exergy (kW)
$\dot{E}x_d$	Exergy destruction rate (kW)
En	Energy (kW)
Ex_{ph}	Physical Exergy (kW)
Ex_{ch}	Chemical Exergy (kW)
MW	Molar Mass (kg/mol)
COP	Coefficient of Performance
η	Efficiency

Subscripts

Abs	Absorber
Cond	Condenser
Evap	Evaporator
Hx	Heat Exchanger
Turb	Turbine

d	Destruction
x	Concentration of the Solution
H_2	Hydrogen
avg	Average
1,2,3..	State Numbers
0	Ambient

Acronyms

SEAC	Single Effect Absorption Chiller
ORC	Organic Rankine Cycle
RSRC	Reheat Steam Rankine Cycle
EES	Engineering Equation Solver
AC	Air Conditioner
WEC	World Energy Council
PEM	Proton Exchange Membrane
AHW	Atomic Hydrogen Welding
CFC	Chlorofluorocarbon

Chapter 1

INTRODUCTION

1.1 Overview

There is no denying the fact that continuous growth of population have been increasing the world's fossil fuel demand and consumption, which, as result, increased the cost of fuel. Moreover, consumption of fossil fuels emits greenhouse gasses (GHGs), which is the main cause of global warming and other environmental problems such as ozone depletion and acid rains.

Therefore, to address the disbenefits and problems regarding the usage of fossil fuels, both environmentally and economically, scientists and engineers have been studying the alternative energy sources extensively over the past few decades not only to meet the energy demands but also to find more environmentally friendly sources of energy.

Renewable energy sources, as an unlimited source, can help to reduce the emissions of greenhouse gasses in the atmosphere and also address the increasing energy demands and diminishing fossil fuel reserves. Many renewable energy sources (RES) have been investigated by the researchers, such as; solar, wind, geothermal, hydropower, salinity gradient, ocean thermal, biomass & biofuel, etc.

One of the most abundant, well operated, highly efficient and reliable and also accessible RESs is biomass fuel. The phrase "biomass", denotes to organic material that has stored energy over the photosynthesis process (Ameri, 2013). Biomass energy is form of energy that is a contained in plants and animals. As of today, wood remains are the greatest source of biomass energy (Chum, 2001).

Approximately 65% of the total CO_2 emissions is comprise of power generation, heating and cooling (Ahmadi, 2013). Combined heat and power (CHP) which can be typified as a simple multi-generational system, meets the main portion of the energy demands, including heating and electricity load. In the integrated multi-generation, waste heat from electricity generation process is utilized in a beneficial heating process, like domestic water heating (DWH) or space heating. Energy efficiency of a cogeneration system is usually between 40–80%. In addition, CHPs have been expanded to tri-generation systems, which generates district cooling as well. Tri-generation plants are very adaptable and versatile which means they could be utilized extensively, like in the residential area, hotels, hospitals, shopping, airports, animal production, and thermo-chemical industries Additionally, to achieve higher amount of overall efficiency, and generate additional products by utilizing single mover, researchers have extended tri-generation to multi-generational power plants. In comparison with other power plant's capabilities, multi-generation systems contain several more cycles such as desalination, drying, and hydrogen producing part. Thus, implementation of multi-generational systems paved the way for waste heat to be reused and recycled in more processes for additional system performance .Hence, because of its high efficiency and less GHGs emissions, multi-generation systems are valuable option for engineers to reflect and research.

1.2 Objectives of the Study

The objective of the present work is to achieve energy efficiency by designing a multi-generation system, where electricity, thermal energy, and hydrogen is generated from a biomass plant that utilizes pine sawdust. It aims to use thermal energy for heating, cooling, and drying purposes.

1.3 Organization of the Thesis

The thesis is arranged as follows:

In chapter 2, the information accessible in the literature is explored to authenticate the nexus of subject, knowledge gap is identifying simultaneously.

In Chapter 3, the model is explained and described in detail.

Chapter 4, justifies the proper mathematical calculation.

In chapter 5, the results are presented and discussed in details.

In chapter 6, the conclusions are presented and some recommendations are made.

Chapter 2

LITERATURE REVIEW

2.1 Introduction

In this chapter, several studies associated with the multi-generation systems have been presented and discussed. One of the approaches in this chapter is to cover the papers, which have been published recently, and incorporated thermodynamic analysis related to the multi-generation system. In addition, the papers aim and methodology is explained in details in following text.

The literature on cogeneration, trigeneration, and multi-generation system using different primary energy sources is reviewed. The multi-generation renewable system is being fed by one or more renewable sources and generating several products. The primary aims of using such cycles are to enhance sustainability, performance and also to decrease expenditure and environmental effects. Thus, because of aforementioned goals, multi-objective power plants are playing a significant role in global warming mitigation.

The potential products of multi-generation systems are consist of electricity, space heating, cooling, drying, electrolyzing, and drinkable water. The use of waste heat from several sub-systems has a potential to be reused in a number of different process. The cycles and processes in a multi-generation power plant can be power

generation, hydrogen oxygen producing unit, heating, air heating, drying, cooling and air-conditioning.

2.2 Cogeneration and Trigeneration Systems

The combination of the ORC-CHP is beneficial for small energy demand. A study about proficiency analyzes and optimization has been done for CHP-ORC (Mago, 2010), which was only applicable for small-scale commercial buildings. After a while, the appraisal of the possibility of emission reduction via using CHP systems studied (Mago, 2010).

Don et al. designed a micro-scale CHP plant combined with SEACS experimentally. They observed the various coefficient of performance for an absorption chiller in the distinct provenance of thermal heating. Scientists (Dong, 2009) have demonstrated a linear relation between the temperature of injected hot water and the performance of SEACS.

Smith et al. (Smith, 2013) have studied performance investigation of a unified cogeneration utility with both electric and thermal energy reservoir in domestic applications. The estimation of the efficiency of systems with heat, cold and power generation, and their assessments related to the overall utilization factor and exergy saving have been developed by Onovwiona et al. (Onovwiona, 2006). By performing the energy assessment of integrated tri-generation systems with heat pumps Miguez et al. (J, 2004), (J P. , 2004) finalized that the presence of heat pump is significant in increasing the efficiency of the cycle. Exergy assessments of an integrated power and cooling plant, in addition, a parametric research for the efficacy of inlet temperature of produced gasses in CC, and gas syntax on exergetic efficiency and utilization

factor, electric-cold factor, and rate of irreversibility for a cogeneration energy system accomplished by Khaliq (Khaliq, 2009).

The first and second law of thermodynamic analyses for a CHP in Ankara and proposition for amendment to diminish the irreversibility in CHP plant (CHPP) were developed by Ganjehkaviri et al. (Ganjehkaviri, 2014). CC, gas turbines (GT) and heat loss recuperation steam generators (HRSG) were primarily origins of destructions, nearly 84% of the total exergy losses of the model.

Ehyaei et al. performed an exergetic assessment on a domestic cogeneration system integrated with a fuel cell (Ehyaei, 2015). Moreover, a complementary study has been done to analyze the effect of various factors in fuel cell design like pressure, temperature, and a relative deep point on the efficiency of the cycle.

The performance assessment of poly-generation systems with supreme efficiency based upon exergy in domestic cases performed (Bingöl, 2011).

Thermo-dynamical analyses of a CHP utility with a molten carbonate fuel cell (MCFC) integrated with a GT system carried out (RS, 2011). They have altered several factors in design to achieve a parametric study about the performance of the system. Based on the assessment the highest production work of the MCFC is nearly 314.3 kW for a working temperature of 923 K. The total utilization factor and exergy efficacy gained for the plant were about 43% and 38%, respectively.

The exergy assessment and parametric research for a hybrid CHP power plant operating an integrated power generation cycle containing of a solid oxide fuel cell

(SOFC) and a GT conducted by Akkaya et al. (AV, 2008). According to the results of SOFC, which is based on an exergy performance factor principle, has substantial benefits since it relatively generated less entropy.

Al-Sulaiman et al. (FA, 2010) noticed an increase in efficiency of approximately 23% through operating a tri-generation system in contrast to SOFC and ORC plant. The maximum efficiencies of tri-generation system are nearly 75%, 72% for heating CHP, 57% for cooling CHP and 47% for power generated were determined, furthermore; as a result, exergy assessment plays a remarkable role for both cogeneration and trigeneration utilities.

For many years, exergo-economics and thermo-economics have been progressively employed by scientist for merging thermodynamics with economics for CHP and power generation.

A power plant which burns coal has been assessed on exergo-economic aspect and carried out by Rosen et al. (MA, 2003), which figured out the enthalpy waste rate to the cost is a crucial factor for system performance.

Trigeneration utilities are the concurrent output of cooling, heating, and power from an ordinary energy resource. It uses heat losses or alternative thermal source from a utility to enhance general heat efficiency, regularly using the free energy accessible with the aid of waste energy. In a trigeneration cycle with rising temperature, heat loss from the origin of the utilities such as GT, diesel motor (Ahmadi, 2011), are movers for combined plants. The output heat of such utilities can be utilized in space heating and residential warm water generation. By running an absorption cooling

plant the heat can also be utilized for cooling. Comparison between energy analysis of tri-generation system and CHP cycle for and ordinary building have been carried out by Pospisil et al. (Pospisil, 2006). Based on the this results, in compare with one generation plant ,cogeneration can rise up the efficiency by 32% and additionally tri-generation cycles can also enhance efficiency to near 40%.

The thermal integration of trigeneration systems observed by Calva et al. (Calva, 2005). They centralized assessment on only trigeneration plants where in a GT is utilized as an origin of cooling also electricity is produced via an ordinary compression refrigeration cycle.

The proficiency assessment of a trigeneration utility containing of a micro GT and an air cooling, indirect fired and ammonia water absorption refrigerator has analyzed by Moya et al. (Moya, 2011). Moreover a parametric study by altering certain design factors, such as the effect of the output power of the micro GT, ambient temperature for the cooling cycle, refrigerator outlet temperature and oil temperature carried out. A novel integrated trigeneration plant containing of a micro GT, an SOFC, and an SEACS suggested by Velumani et al. (Velumani, 2010). The results demonstrated that the sustainability index of this plant is near to 44%.

The proficiency of an integrated trigeneration plant with a microscopic turbine and a tiny solar collector studied by Buck and Fredmann (Buck, 2007). Based on the researcher’s recommendation using the double effect absorption cooling system (DEACS), has greater thermal efficiency in contrast to the SEACS. Exergy is a beneficial method for defining the losses, which become visible in the formation of both exergy destructions rate and waste exergy rate (Dincer, 2012).

Thusly, exergy can help with design techniques and rules for more powerful utilization of energy assets and advances. Recently, exergy assessment has turned into an extremely well-known device for dissecting heating systems. A few reviews have exerted exergy analysis to CHP and trigeneration power plant integrated with IC motors.

2.3 Multi-generation Energy

A system with a unique source of energy, which produces more than three distinct product such as hot water, hydrogen, and drinkable water, is named multi-generation energy utility. The significance of these plants is the possibility to use in domestic areas as well as power plants and places where needed the several outputs. Based on the location and needs of the usage, which is a primary factor in designing the multi-generation, it is possible to design more efficient cycles.

A detailed thermodynamic pattern for an integrated energy system carried out by Hosseini et al. (Hosseini, 2011). The model which deliberated contains a GT, an SOFC unit, and a desalination to generate cooling, power, heat, and drinkable water. A parametric study has been done to analyze the variation of various main design factors with the system efficacy. According to results, the combined system could enhance the system performance by more than 24% in contrast of a one-generation plant.

A modern trigeneration utility containing of a GT, a heat recovery, and an SEACS and an ORC unit studied by Ahmadi et al. (Ahmadi, 2011). Moreover, a parametric research to analyze the efficiencies, environmental impact, sustainability index, specific CO_2 emission, overall utilization factor, demand loads and cost of

environmental impact carried out by them. According to the outcomes of the assessment the system performance is completely influenced by pressure proportion, the inlet temperature and the efficiency for the GT.

A performance analysis of a PV/T and triple efficacy absorption refrigeration plant, for generating cooling and hydrogen carried out by Ratlamwala et al. (Ratlamwala, 2011). Besides an unabridged parametric research, in further study, the implementation of a unique integrated geothermal plant for multi-generation, according to a geothermal double flash power unit, an electrolyzer unit and a quadruple effect absorption cooling system (QEACS), analyzed by Ratlamwala et al. (Dincer I, Gadalla M:., 2012). Augmenting the thermodynamical properties of the geothermal principal temperature, mass flow rate, and pressure amount was apperceived to raise the hydrogen production rate and generated electricity.

A thermodynamic assessment of a multi-generation utility integrated with solar collectors and electrolyzer carried out by Ozturk (Ozturk, 2012). This system contains four units, steam Rankine cycle, ORC, SEACS, and electrolyzer. The exergy efficiency and irreversibility rate for the subsections and the whole plant demonstrate that the solar dish has the greatest irreversibility amount between main components of the multi-objective utility.

An energy and exergy analyses of multi-generation system based on renewable energy, taking into account multiple options for producing such outputs are illustrated in previous multi- objective system (Dincer, 2012).

Ahmadi et al. (Ahmadi P, 2012) carried out the exergy and environmental impact assessment of an ORC integrated with GT as modern multi-generation to yield heating, hot water, cooling, and electricity. The analyzed system contains a GT cycle, an ORC unit, an SEACS and a domestic water heater.

Ahmadi et al. optimized a multi-generation plant in accordance with exergy analysis (Ahmadi P, 2012). The system contains a GT as the prime mover to generate residential demand of power, hot air, and warm water and conditioned air.

Thermodynamic assessments is performed for generating hydrogen by gas turbine modular helium reactor/organic Rankine cycle (GTMHR/ORC) integrated with a proton exchange membrane electrolyzer (Nami, 2016). An extensive parametric research had carried out, and the efficacy of various factors such as compressor pressure ratio and pinch point temperature difference in the evaporators on the exergy efficiency, the amount of generated hydrogen and sustainability index of the combined cycles were performed. To achieving the highest exergy performance, the Engineering Equation Solver (EES) software has been used. According to the outcomes, the exergy efficiency diversity among the integrated utility and GTMHR system rises by growth in pressure proportion. Moreover, it is apperceived that the amount of generated hydrogen rises with increasing turbine inlet temperature and takes the highest extent with alter in evaporators' temperature. Based on the results of this research alter in the evaporator's temperature optimizes both exergy efficiency and amount of generated hydrogen. By this optimized condition, the exergy efficiency, amount of generated hydrogen and sustainability index are 49.21, 56.2 kg/h and 1.972, respectively.

As respects as, the wastes of wood industries and agriculture sector make the majority of biomass fuel. Biomass is one of the cheapest, most accessible and capable alternative energy origins for fossil fuels. Biomass is a complex of some materials that are applicable in many ways leading to various outputs (H.L. Chum, 2001), Pyrolysis, gasification, and combustion, are the conventional processes, which are used to extract their thermo-chemical energy (Ferreira, 2001). Combustion is the most efficient and popular one among them (Franco, 2005) cause of having less costly drying processes and being more easily usable. So biomass combustion is an appropriate source of a food for utility. Integrated turbine combustion cycle is one of the most famous available methods in generating electricity from biofuel.

Chapter 3

DESCRIPTION OF THE SYSTEM

In the present work, a multiobjective energy plant is modeled and analyzed. Figure 3.1 represents the concept of the multi-generation plants, which is used extensively to produce electricity, space heating, hot water, air-conditioning, and hydrogen. One of the most important attributes of the present research is the usage of biomass as a source of energy. The system consist of different cycles to use the primary energy as efficiently as possible.

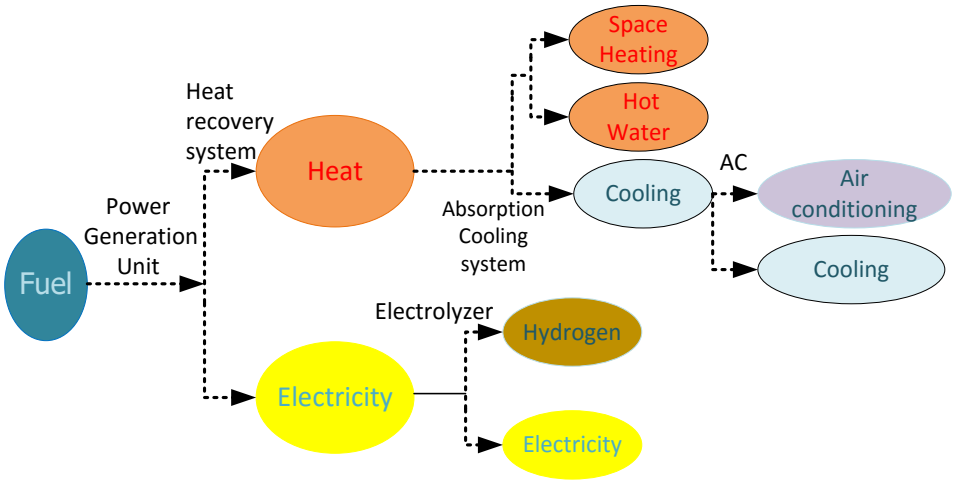

Figure 3.1: A typical multi-objective system

Since organic materials constitute the biomass resource, it can be renewed naturally (Cohce, 2011). Biomass includes all the living matters on the earth, and is capable of being utilized either directly, or converted into different forms such as biofuels (Cohce, 2011). The conventional and direct way of utilizing biomass is to through burning it to produce heat and electricity. In addition, the two other indirect method for utilizing biofuel, which is through thermo-chemical conversion process, are pyrolysis and gasification. For large-scale utilization, these technologies are not economically feasible due to their lack of equipment development (Lian, 2010). Some researchers have worked on cogeneration power plant based on biomass (Chum, 2001), (Dong, 2009). They applied biomass combustion technologies in various industries such as paper, rice, wood, sugar, and palm oil as a waste disposal, which are consistent with energy conservation principle (Mujeebu, 2009).

Figure 3.2 shows the schematic of the modeled multi-generation plant, which obeys the principles of Figure 3.1. As it has shown, the integrated system comprising of a biomass combustion chamber (CC), a reheat Rankine cycle (RRC) and organic Rankine cycle (ORC) to generate electricity, a single-effect absorption cooling system (SEACS) for cooling load, an air conditioner (AC) and an electrolyzer to

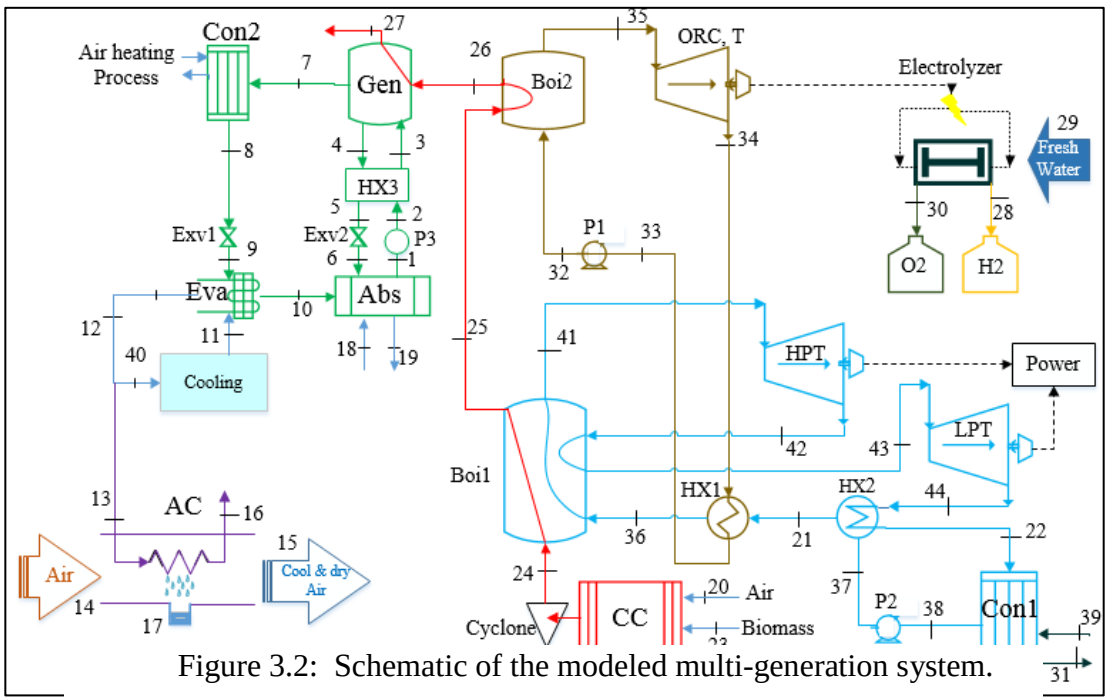

Figure 3.2: Schematic of the modeled multi-generation system.

produce hydrogen.

The pine sawdust is a kind of accessible biomass, which is intended to burn in the CC as the input fuel of the system. A cyclone operated in exit of the CC to absorb the ashes that exist in the exhaust gasses. The hot exhaust gasses produced by combustion process are initially entering to the RSRC unit then proceeding to ORC cycle (boiler 1 and boiler 2 respectively) and finally arriving to the generator in the SEACS, to provide the required heat for evaporation process. The waste heat from the ORC is utilized to preheat water flow that is used in RSRC for the heating process (exchanger1 (HX1)). To operate ORC with high efficiency, it should work in high critical temperature (Ziher, 2006). N-heptane has chosen as organic fluid for ORC, which its critical temperature is reasonably high (540.1 K) (Kay, 1938). Saturated liquid n-heptane enters the pump 1 at state 33 then Pump1 increases the pressure of n-heptane and subsequently high-pressure n-heptane enters the boiler 2 at state 32.

The ORC cycle produces electricity, which is supplied to drives a PEM electrolyzer. Since the exhaust gasses leaving the generator has not considerable energy anymore, they are released to the environment.

As seen in figure 3.2, biofuel and air enter the CC at state 23 and state 20 respectively. To decrease the amount of harmful particles, such as ash, hot gasses that produced in CC, are passing through the cyclone. Hot flue gasses enter boiler to produce superheated steam at state 41 and 43 to transfer towards the high-pressure turbine (HPT) and low-pressure turbine (LPT) to produce shaft work. The superheated steam at states 42 and 44 are expanded to rotate the generators, and the

used-steam from the low-pressure turbine passes through the heat exchanger (HX2) then enters the condenser for condensation process and water heating process simultaneously. Saturated water leaves the condenser 1 and enters the pump 2 at state 38. The pressure of water is increased by pump 1, and high-pressure water enters the heat exchanger (HX1) at state 21 to raise the temperature. High-pressure water after been preheated at HX1 enters to the boiler 1 at state 36 to close the RSRC cycle.

Weak LiBr/Water solution at state one is sent to the heat exchanger (HX3) by pump 3 for the preheating process in HX3. Weak LiBr/Water solution enters the generator to boil. In the generator, the weak solution of LiBr/Water is heated to produce water then the concentrated LiBr/Water solution is sent back to HX3. Pure water in the superheated condition leaves the generator and enters in to the condenser 2. After condensation, the saturated liquid water enters to the expansion valve. In the expansion valve, throttling process takes place on the water, and pressure is decreased. Mix saturated vapor leaves the expansion valve and enters the evaporator to absorb heat from embedded space. Since the evaporator pressure is low, by absorbing heat , mix-saturated vapor is converted to superheated vapor in the evaporator outlet.

The cooling generated at the evaporator is partly used for cooling a building such as an office and the rest is sent to the air-conditioner for the preparation of cool dry air. Warm and humid air enters AC at state 14 and after absorption of its moisture by AC (state 7), dry and cold air forms at state 15 and is sent to the buildings. Table 1 describes each state of the systems in more detail.

Table 1: Description of the multi-generation system

State	Description	State	Description
1	Weak solution LiBr/Water inlet to pump	23	Biomass fuel inlet to the combustion chamber
2	Weak solution LiBr/Water Inlet to HX	24	Hot flue gasses leaves the combustion chamber
3	Weak solution LiBr/Water inlet to generator	25	Hot flue gasses inlet to the boiler
4	Strong solution LiBr/Water leaves the generator	26	Hot flue gasses inlet to the generator
5	Strong solution leaves the HX	27	Exhausted gasses is released to the environment
6	Strong solution LiBr/Water leaves the expansion valve	28	Produced hydrogen leaves the electrolyzer
7	Water vapor leaves the generator	29	Water inlet to the electrolyzer
8	Saturated liquid water leaves the condenser	30	Produced oxygen leaves the electrolyzer
9	Mix saturated vapor inlet to the evaporator	31	Hot water outlet from the condenser
10	Saturated vapor inlet to absorber	32	ORC fluid inlet to the boiler
11	Warm air inlet to the evaporator	33	ORC fluid inlet to the pump
12	Chilled air outlet from the evaporator	34	ORC fluid leaves the ORC turbine
13	Chilled air outlet from the evaporator	35	Superheated n-Heptane inlet to the ORC turbine
14	Warm and humid air inlet to the AC	36	Liquid water inlet to the boiler
15	Cooled & dry air outlet from the AC	37	Liquid water inlet to the heat exchanger
16	Warm air outlet from the AC	38	Liquid water inlet to the pump
17	Absorbed moisture in the AC	39	water inlet to the condenser
18	Cold water inlet to absorber	40	Chilled air
19	Hot water outlet from the absorber	41	Superheated steam inlet to the high-pressure turbine
20	Air inlet the biomass combustion chamber	42	Superheated steam leaves the high-pressure turbine
21	Saturated liquid water leaves the heat exchanger	43	Superheated steam inlet to the low-pressure turbine

22	Saturated liquid water inlet to the condenser	44	Superheated steam leaves the low-pressure turbine

Chapter 4

METHODOLOGY

4.1 Thermodynamic Analysis

To examine the proposed integrated system, a complete analysis based on the mass balance, first and second law of thermodynamic have been performed. These evaluations represent the energy performance, exergy performance and environmental impacts and also sustainability index, for the multi-objective utility.

The whole body of the system has been categorized and sorted in a way that each cycle and component of system have been analyzed independently. Furthermore, the efficiency of the RSRC, ORC, PEM electrolyzer, AC and coefficient of performance of SEACS have been computed.

The main assumptions are:

1. Every parts and equipment of utility operate in steady conditions.

2. Heat lost pressure drops in all the pipes and equipment considered to be negligible.

3. The environment state is specified to have a pressure of P_0 = 100kPa and a temperature of T_0 = 293.15 K.

4. Produced gasses and air are considered as an ideal gas mixtures. (Since these gasses are in low pressure and high temperature, this assumption is reasonable.)

5. The throttling process (expansion valve 1 and expansion valve 2) is conducting in isenthalpic conditions.

Mass balance, energy, exergy, exergo-environmental, have been represented below.

4.1.1 Biomass Combustion Chamber

As shown in figure 4.1, air and biomass enter the CC at state 20 and state 23, respectively.

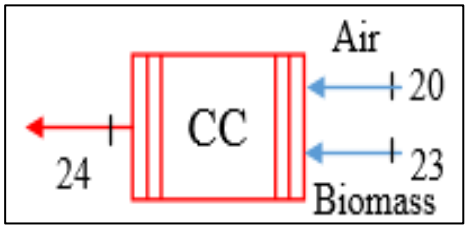

Figure 4.1: Schematic of the combustion chamber

The composition of pine sawdust (biofuel of the system) is described in Table 2.

Table 2: Composition of pine sawdust (Ahmadi, 2013)

Composition	**Value (%)**
Moisture (percentage in weight)	10
Element content (percentage in dry sample of pine sawdust)	
Sulfur (S)	0.57
Hydrogen (H)	7.08
Carbon (C)	50.54
Oxygen (O)	44.11

The chemical calculations were carried out to find composition of pine sawdust, which result in $C_5H_8O_3$ as the chemical formula for chosen pine sawdust.

The chemical equation of pine sawdust combustion is:

$$C_xH_yO_z + \omega H_2O + \lambda(O_2 + 3.76N_2) \rightarrow aCO_2 + bH_2O + cN_2 \quad (1)$$

where, ω is the amount of moisture in the fuel. The molar mass of the fuel can be obtained from:

$$\dot{n}C_xH_yO_z = \frac{\dot{m}_{biomass}}{M_{C_xH_yO_z}} \quad (2)$$

where, $M_{C_xH_yO_z}$ is the molar mass of the fuel. The coefficients of Eq. (1) are specified from element balances:

$$a = x \quad (3)$$

$$b = \frac{y + 2\omega}{2} \quad (4)$$

$$c = \frac{79}{21}\lambda \quad (5)$$

where:

$$\lambda = \frac{2a + b - \omega - z}{2} \quad (6)$$

Energy balance has been conducted to find the temperature of product exiting from CC:

$$\bar{h}C_xH_yO_z^{,23} + \omega\bar{h}H_2O^{,20} + \lambda\bar{h}O_2^{,20} + 3.76\lambda hN_2^{,20} = ahCO_2^{,24} + bhH_2O^{,24} + c\bar{h}N_2^{,24} \quad (7)$$

where, $\bar{h}C_xH_yO_z$ is defined as (Basu, 2006):

$$\bar{h}C_xH_yO_z^{,23} = x\bar{h}CO_2^{,24} + \frac{y}{2}\bar{h}H_2O(l)^{,23} + \overline{LHV}_{biomass}M_{C_xH_yO_z} \quad (8)$$

For dry biofuels, sulphur (S) and Nitrogen (N) content are very low. So due to calculating low heat value (LHV) for fuel with $C_xH_yO_z$ formula, this calculation can be used:

$$\overline{LHV}_{dry} = \frac{400000 + 100600y - \frac{z/x}{1+0.5(y/z)}\left(117600 + 100600(y/x)\right)}{12 + (y/x) + 16(z/x)} \quad (9)$$

The LHV for humid biofuel (Basu, 2006):

$$\overline{LHV}_{mois} = \left[1 - \mu_m - H_u\right]\overline{LHV}_{dry} - 2500H_u \quad (10)$$

where H_u and μ_m are the content of humidity and mineral matter in biofuel. By the temperatures at states 20 and 23, Eq. (7) can be solved to find the amount of temperature at state 24.

By applying Eq. (9) and Eq. (10) the LHV of pine sawdust was found 9579 kJ/kG

LHV= 9579

4.1.2 Organic Rankine Cycle

ORC turbine, ORC heat exchanger, ORC boiler (boiler 2), and ORC pump are the components of ORC unit. (See the figure 3.2).

For Organic Rankine Cycle, Turbine

Schematic of the ORC turbine has been shown in figure 4.2.

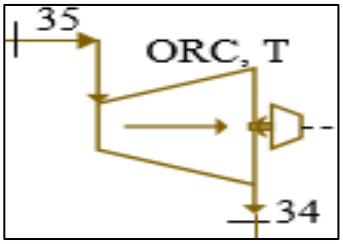

Figure 4.2: Schematic of the ORC, T

The following equation are used for ORC turbine:

Mass balance:

$$\dot{m}_{34} = \dot{m}_{35} \tag{11}$$

where $\dot{m}_{34}$ and $\dot{m}_{35}$ are the inlet and outlet mass flow rates of superheated n-heptane going through the turbine.

$$\eta_{ORC,T} = \frac{\dot{W}_a}{\dot{W}_s} \tag{12}$$

where $\dot{W}_a$, $\dot{W}_s$, $\eta_{ORC,T}$, are the actual work, isentropic work, and isentropic efficiency of the turbine.

Energy balance:

$$\dot{W}_{ORC,T} = \dot{m}_{35}\left(h_{35} - h_{34}\right)\eta_{ORC,T} \tag{13}$$

where $\dot{W}_{ORC,T}$, h_{35} and h_{34} are the produced power by ORC turbine, in the inlet and outlet enthalpy of the superheated n-heptane going through the ORC turbine, respectively.

Exergy balance:

$$\dot{E}x_{Des,ORC,T} = Ex_{35} - Ex_{34} - \dot{W}_{Turbine} \quad (14)$$

where, Ex_{35} , Ex_{34} and $\dot{E}x_{Des,ORC,T}$ are the representative of the exergy destruction rate, the inlet and outlet exergy of the superheated n-heptane going through the turbine, respectively.

For Heat Exchanger 1

Schematic of the HX1 has been shown in figure 4.2.

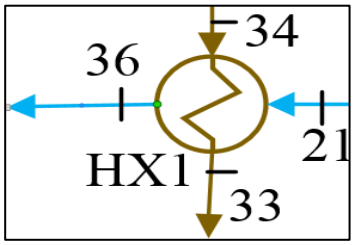

Figure 4.3: Schematic of the HX1

The following equations are used for heat exchanger (HX1):

Mass balance:

$$\dot{m}_{34} = \dot{m}_{33} \quad (15)$$

where $\dot{m}_{33}$ is the outlet mass flow rate of saturated n-heptane of heat exchanger 1.

$$\dot{m}_{21} = \dot{m}_{36} \quad (16)$$

where $\dot{m}_{21}$ and $\dot{m}_{36}$ is the inlet and outlet mass flow rate of saturated steam going through the heat exchanger 1.

Energy balance:

$$\dot{m}_{34} h_{34} + \dot{m}_{21} h_{21} = \dot{m}_{36} h_{36} + \dot{m}_{33} h_{33} \quad (17)$$

where, h_{34} and h_{33} are the inlet and outlet enthalpy of the saturated n-heptane, h_{21} and h_{36} are the inlet and outlet enthalpy of the saturated steam going through the heat exchanger 1.

Exergy balance:

$$Ex_{34} - Ex_{33} = Ex_{36} - Ex_{21} + \dot{E}x_{Des,HX1} \quad (19)$$

where Ex_{34} and Ex_{34} are the inlet and outlet exergy of the saturated n-heptane, Ex_{21} and Ex_{36} are the inlet and outlet exergy of the saturated steam going through the heat exchanger 1, and $\dot{E}x_{Des,HX1}$ are the exergy destruction rate of heat exchanger 1.

For Boiler 2

Schematic of the boiler 2 has been shown in figure 4.4.

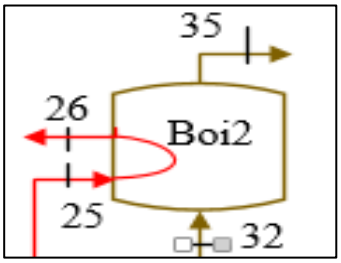

Figure 4.4: Schematic of the Boiler 2

The following equations are used for boiler 2:

Mass balance:

$$\dot{m}_{25} = \dot{m}_{26} \tag{20}$$

where $\dot{m}_{25}$ and $\dot{m}_{26}$ are the inlet and outlet mass flow rate of exhaust gasses going through the boiler 2.

$$\dot{m}_{35} = \dot{m}_{32} \tag{21}$$

where $\dot{m}_{35}$ is the inlet mass flow rate of saturated liquid n-heptane, and $\dot{m}_{32}$ is the outlet mass flow rate of superheated n-heptane, going through boiler 2.

Energy balance:

$$\dot{m}_{35} h_{35} - \dot{m}_{32} h_{32} = \dot{m}_{26} h_{26} - \dot{m}_{25} h_{25} \tag{22}$$

$$\dot{Q}_{in,Boi2} = \dot{m}_{35} h_{35} - \dot{m}_{32} h_{32} \tag{23}$$

where, h_{35} , h_{32} and $\dot{Q}_{in,Boi2}$ are the inlet and outlet enthalpy of mass flow rate going through boiler 2.

Exergy analysis:

$$\dot{E}x_{termal,Boi2} = \dot{Q}_{Boi2}(1 - T_0 / T_{ave,Boi2}) \tag{24}$$

$$T_{ave,Boi2} = (T_{25} + T_{26} + T_{32} + T_{35}) / 4 \tag{25}$$

$$Ex_{32} + Ex_{25} = Ex_{35} + Ex_{26} + \dot{E}x_{Des,Boi2} \tag{26}$$

where $\dot{E}x_{Des,Boi2}$ is the exergy destruction of boiler 2, Ex_{32} and Ex_{35} are the inlet and outlet exergy of n-heptane, Ex_{25} and Ex_{26} are the inlet and outlet exergy of exhaust gasses, going through boiler 2.

For Pump 1

Schematic of the pump 1 has been shown in figure 4.4.

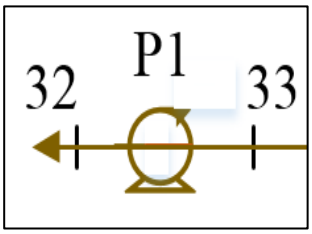

Figure 4.5: Schematic of the pump 1

The following equations are used for pump 1:

Mass balance:

$$\dot{m}_{32} = \dot{m}_{33} \tag{27}$$

where $\dot{m}_{33}$ and $\dot{m}_{32}$ are the inlet and outlet mass flow rate of liquid n-heptane going through pump 1.

Energy balance:

$$\dot{W}_{P1} = \dot{m}_{32}\, v_{32} \left(P_{32} - P_{33}\right) / \eta_{s,P1} \tag{28}$$

$$\eta_{s,P1} = \frac{\dot{W}_s}{\dot{W}_a} \tag{29}$$

where, $\dot{W}_{P1}$, P_{32}, P_{33}, v_{32}, and $\eta_{s,P1}$ are the produced power by pump 1, inlet and outlet pressure of the n-heptane going through the pump 1, inlet specific volume of n-heptane, isentropic efficiency, and exergy destruction in pump 1, respectively.

Exergy balance for pump 1:

$$\dot{E}x_{Des,P1} + Ex_{32} = Ex_{33} + \dot{W}_{P1} \tag{30}$$

where, $\dot{E}x_{Des,P1}$ is the representative of exergy destruction rate in pump 1.

4.1.3 Reheat Steam Rankine Cycle

The RSRC cycle here has 6 major components as follows:

RSRC boiler (boiler 1), RSRC high-pressure turbine (HPT), RSRC low-pressure turbine (LPT), RSRC heat exchanger (HX2), RSRC condenser (condenser 1), and RSRC pump (P2).

For Pump 2

Schematic of the pump 2 has been shown in figure 4.6.

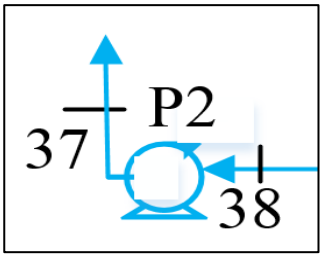

Figure 4.6: Schematic of the pump 2

The following equations are used for pump 2:

Mass balance:

$$\dot{m}_{37} = \dot{m}_{38} \tag{31}$$

where $\dot{m}_{38}$ and $\dot{m}_{37}$ are the inlet and outlet mass flow rate of liquid water going through the heat pump 2.

Energy balance:

$$\dot{W}_{P2} = \dot{m}_{37} v_{37} \left(P_{37} - P_{38}\right) / \eta_{P2} \tag{32}$$

$$\eta_{P2} = \frac{\dot{W}_s}{\dot{W}_a} \tag{33}$$

where, $\dot{W}_{P2}$, P_{38}, P_{37}, v_{37}, and $\eta_{s,P2}$ are the produced power by pump 2, inlet and outlet pressure of the liquid water going through the pump 2, inlet specific volume liquid water, isentropic efficiency, and exergy destruction in pump 2, respectively.

Exergy destruction:

$$\dot{E}x_{Des,P2} + Ex_{37} = Ex_{38} + \dot{W}_{P2} \tag{34}$$

where Ex_{38}, Ex_{37}, and $\dot{E}x_{Des,P1}$ are the representative of inlet and outlet exergy of liquid water, and exergy destruction rate of pump 2, respectively.

For Heat exchanger 2

Schematic of the HX2 has been shown in figure 4.7.

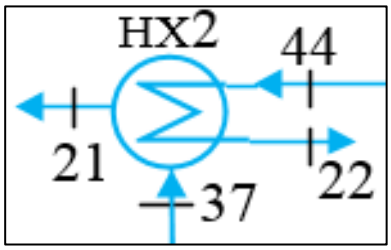

Figure 4.7: Schematic of the heat exchanger 2

Mass balance:

$$\dot{m}_{44} = \dot{m}_{22} \tag{35}$$

where $\dot{m}_{44}$ is inlet mass flow rate of superheated steam, and $\dot{m}_{22}$ is outlet mass flow rate of saturated liquid going through the heat exchanger 2.

$$\dot{m}_{21} = \dot{m}_{37} \tag{36}$$

where, $\dot{m}_{37}$ and $\dot{m}_{21}$ are the inlet mass flow rate of liquid water, going through the heat exchanger 2.

Energy balance:

$$\dot{m}_{44}\, h_{44} - \dot{m}_{22}\, h_{22} = \dot{m}_{21}\, h_{21} - \dot{m}_{37}\, h_{37} \tag{37}$$

where, h_{37} and h_{44} are the inlet enthalpy of the liquid water, h_{21} and h_{22} are the outlet enthalpy of the saturated steam going through the heat exchanger 2.

Exergy balance:

$$Ex_{37} + Ex_{44} = Ex_{22} + Ex_{21} + \dot{E}x_{Des,HX\,2} \tag{38}$$

where Ex_{37} and Ex_{44} are the inlet exergy of the liquid water, Ex_{21} and Ex_{22} are the outlet exergy of the saturated steam going through the heat exchanger 2. $\dot{E}x_{Des,HX1}$ are the representative of the exergy drstruction rate in heat exchanger 2.

For High Pressure Turbine

Schematic of the HPT has been shown in figure 4.7.

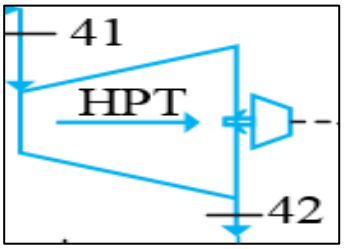

Figure 4.8: Schematic of the HPT

The following equations are used for HPT:

Mass balance:

$$\dot{m}_{41} = \dot{m}_{42} \tag{39}$$

where $\dot{m}_{41}$ and $\dot{m}_{42}$ are the inlet and outlet mass flow rates of superheated steam going through the HPT.

Energy balance:

$$\dot{W}_{HPT} = \dot{m}_{41}\left(h_{41} - h_{42}\right) \cong \dot{m}_{41}\left(h_{41} - h_{42}\right)\eta_{s,HPT} \tag{40}$$

where $\dot{W}_{HPT}$, h_{41} and h_{42} are the produced power by HPT, inlet and outlet enthalpy of the superheated steam going through the HPT. $\eta_{s,HPT}$ is the isentropic efficiency of HPT.

Exergy balance:

$$\dot{E}x_{Des,HPT} = Ex_{41} - Ex_{42} - \dot{W}_{HPT} \tag{41}$$

where Ex_{41} and Ex_{42} are the inlet and outlet exergy of superheated steam going through the HPT, and drstruction rate in HPT, respectively.

For Low Pressure Turbine

Schematic of the LPT has been shown in figure 4.8.

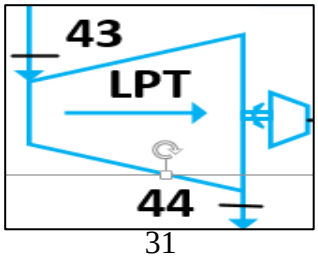

Figure 4.9: Schematic
of the LPT

The following equations are used for LPT:

Mass balance:

$$\dot{m}_{43} = \dot{m}_{44} \tag{42}$$

where $\dot{m}_{43}$ and $\dot{m}_{44}$ are the inlet and outlet mass flow rates of superheated steam going through the LPT.

Energy balance:

$$\dot{W}_{LPT} = \dot{m}_{43}\left(h_{43} - h_{44}\right) \cong \dot{m}_{43}\left(h_{43} - h_{44}\right)\eta_{LPT} \tag{43}$$

where $\dot{W}_{LPT}$, h_{43} and h_{44} are the produced power by LPT, inlet and outlet enthalpy of the superheated steam going through the LPT. $\eta_{s,LPT}$ is the isentropic efficiency of LPT.

Exergy analysis:

$$\dot{E}x_{Des,LPT} = Ex_{43} - Ex_{44} - \dot{W}_{LPT} \tag{44}$$

where Ex_{43} and Ex_{44} are the inlet and outlet exergy of superheated steam going through the LPT, and destruction rate in LPT, respectively.

For Condenser 1

Schematic of the condenser 1 has been shown in figure 4.9.

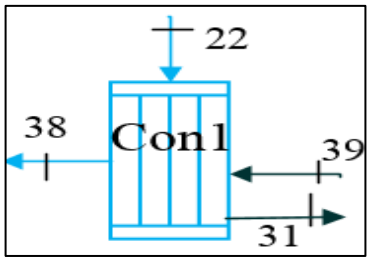

Figure 4.10: Schematic of the Condenser 1

The following equations are used for condenser 1:

$$\dot{m}_{39} = \dot{m}_{31} \tag{45}$$

$$\dot{m}_{38} = \dot{m}_{22} \tag{46}$$

where $\dot{m}_{22}$ and $\dot{m}_{39}$ are the inlet mass flow rate of liquid water, $\dot{m}_{38}$ and $\dot{m}_{31}$ are the outlet mass flow rate of liquid water going through the condenser 1.

Energy analysis:

$$\dot{m}_{22} h_{22} - \dot{m}_{38} h_{38} = \dot{m}_{31} h_{31} - \dot{m}_{39} h_{39} \tag{47}$$

$$\dot{Q}_{out,Con1} = \dot{m}_{31} h_{31} - \dot{m}_{39} h_{39} \tag{48}$$

where, h_{22} and h_{39} are the inlet enthalpy of the liquid water, h_{38} and h_{31} are the outlet enthalpy of the liquid water going through the heat condenser 2. $\dot{Q}_{out,Con1}$ is the removed heat from condenser 1.

Exergy analysis:

$$\dot{E}x_{termal,Con1} = \dot{Q}_{Con1}(1 - T_0 / T_{ave,Con1}) \tag{49}$$

$\dot{E}x_{termal,Con1}$ is the thermal exergy removed from condenser 1, and $T_{ave,Con1}$ is the condenser 1 average temperature, can be obtained by Eq. (50):

$$T_{ave,Con1} = (T_{22} + T_{31} + T_{38} + T_{39})/4 \quad (50)$$

$$Ex_{22} - Ex_{38} = \dot{E}x_{termal,Con1} + \dot{E}x_{Des,Con1} \quad (51)$$

where Ex_{22} and Ex_{38} are the inlet and outlet exergy of liquid water going through the condenser 1. and $\dot{E}x_{Des,Con1}$ is the destruction rate in condenser 1.

For Boiler 1

Schematic of the boiler 1 has been shown in figure 4.10.

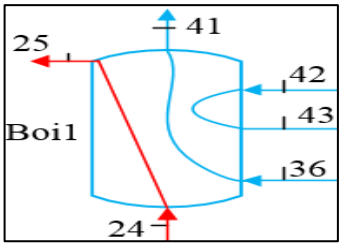

Figure 4.11: Schematic of the Boiler 1

The following equations are used for boiler 1:

Mass balance:

$$\dot{m}_{36} = \dot{m}_{41} = \dot{m}_{42} = \dot{m}_{43} \quad (52)$$

$$\dot{m}_{25} = \dot{m}_{24} \quad (53)$$

where $\dot{m}_{24}$ and $\dot{m}_{25}$ are the inlet and outlet mass flow rate of exhaust gasses going through the heat boiler 1.

Energy analysis:

$$\dot{m}_{36}[(h_{41} - h_{36}) + (h_{43} - h_{42})] = \dot{m}_{24}(h_{24} - h_{25}) \quad (54)$$

$$\dot{Q}_{in,Boi1} = \dot{m}_{41}[(h_{41} - h_{36}) + (h_{43} - h_{42})] \quad (55)$$

where h_{24} and h_{25} are the inlet and outlet enthalpy of exhaust gasses going through the heat boiler 1. $\dot{Q}_{in,Boi1}$ is the injected boiler 1.

Exergy analysis:

$$\dot{E}x_{termal,Boi1} = \dot{Q}_{Boi1}(1 - T_0 / T_{ave,Boi1}) \quad (56)$$

$\dot{E}x_{termal,Boi1}$ is the injected thermal exergy to boiler 1, and $T_{ave,Boi1}$ is the boiler 1 average temperature, can be obtained by Eq. (57):

$$T_{ave,Boi1} = (T_{25} + T_{24} + T_{36} + T_{41} + T_{42} + T_{43}) / 6 \quad (57)$$

$$Ex_{24} - Ex_{25} = Ex_{41} + Ex_{43} - Ex_{36} + Ex_{42} + \dot{E}x_{Des,Boi1} \quad (58)$$

where, $\dot{E}x_{Des,Boi1}$ is the exergy destruction of boiler 1. Ex_{24} and Ex_{25} are the inlet and outlet exergy of exhaust gasses, going through the boiler 1.

4.1.4 Single Effect Absorption Cooling System

The SEACS here has 8 major components as follows:

SEACS generator (Gen), SEACS condenser (Con1), SEACS absorber (Abs), SEACS heat exchanger (HX3), SEACS expansion valves (Exv1 and Exv2), SEACS pump (P3), and SEACS evaporator (Eva).

For Generator:

Schematic of the generator has been shown in figure 4.11.

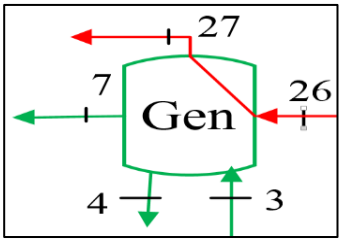

Figure 4.12: Schematic of the generator

The following equations are used for generator:

Mass balance:

$$\dot{m}_4 + \dot{m}_7 = \dot{m}_3 \tag{59}$$

where $\dot{m}_7$ is the outlet mass flow rate of superheated steam, $\dot{m}_3$ is the inlet mass flow rate of weak solution, $\dot{m}_4$ is the outlet strong solution going through the generator.

$$\dot{m}_{27} = \dot{m}_{26} \tag{60}$$

where $\dot{m}_{26}$ and $\dot{m}_{27}$ are the inlet and outlet mass flow rate of exhaust gasses going through the generator.

Concentration balance:

$$\dot{m}_3 x_3 = \dot{m}_4 x_4 \tag{61}$$

where, X_3 and X_4 are the inlet and outlet concentration of solution going through the generator.

Energy balance:

$$\dot{m}_7 h_7 + \dot{m}_4 h_4 - \dot{m}_3 h_3 = \dot{m}_{27} h_{27} - \dot{m}_{26} h_{26} \tag{62}$$

where h_7 is the outlet enthalpy of superheated steam, leaves generator, h_3 and h_4 are the inlet and outlet enthalpy of solution, going through the generator, h_{26} and h_{27} are the inlet and outlet enthalpy of exhaust gasses going through the generator.

Injected heat ($\dot{Q}_{in,Gen}$) can be obtained from Eq. (63)

$$\dot{Q}_{in,Gen} = \dot{m}_{26}(h_{26} - h_{27}) \tag{63}$$

Exergy analysis:

$$\dot{E}x_{termal,Gen} = \dot{Q}_{Gen}(1 - T_0 / T_{ave,Gen}) \tag{64}$$

where, $\dot{E}x_{termal,Gen}$ and $T_{ave,Gen}$ are the representative of injected thermal heat to the generator and average temperature of the generator that is calculated by:

$$T_{ave,Gen} = (T_{26} + T_{27} + T_3 + T_4 + T_7)/5 \tag{65}$$

$$Ex_{26} - Ex_{27} = \dot{E}x_{termal,Gen} + \dot{E}x_{Des,Gen} \tag{66}$$

where Ex_{26}, Ex_{27} and $\dot{E}x_{Des,Gen}$ are the representative of the inlet and outlet exergy of exhaust gasses going through the generator, and exergy destruction rate in generator, respectively.

For Absorber:

Schematic of the absorber has been shown in figure 4.13.

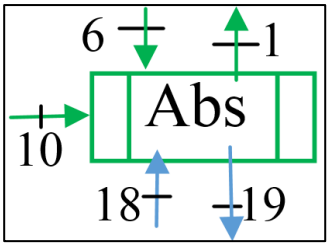

Figure 4.13: Schematic of the absorber

The following equation are used for absorber:

Mass balance:

$$\dot{m}_6 + \dot{m}_{10} = \dot{m}_1 \tag{67}$$

where $\dot{m}_{10}$ is the inlet mass flow rate of low-pressure superheated steam, $\dot{m}_1$ and $\dot{m}_6$ is the inlet and outlet mass flow rate of solution going through the absorber.

$$\dot{m}_{19} = \dot{m}_{18} \tag{68}$$

where, $\dot{m}_{18}$ and $\dot{m}_{19}$ are the inlet and outlet mass flow rates of water going through the absorber.

Concentration balance:

$$\dot{m}_1 x_1 = \dot{m}_6 x_6 \tag{69}$$

where, X_1 and X_6 are the inlet and outlet concentration of solution going through the absorber.

Energy balance:

$$\dot{m}_6 h_6 + \dot{m}_{18} h_{18} + \dot{m}_{10} h_{10} = \dot{m}_{19} h_{19} - \dot{m}_1 h_1 \tag{70}$$

$$\dot{Q}_{out,Abs} = \dot{m}_{10} h_{10} + \dot{m}_6 h_6 - \dot{m}_1 h_1 \tag{71}$$

where h_1 and h_6 are the inlet and outlet enthalpy of solution, h_{10} is the inlet enthalpy of superheated steam, h_{18} and h_{19} are the inlet and outlet enthalpy of water going through the absorber. $\dot{Q}_{out,Abs}$ is the removed heat from the absorber.

Exergy analysis:

$$\dot{E}x_{termal,Abs} = \dot{Q}_{Abs}(1 - T_0 / T_{ave,Abs}) \tag{72}$$

where, $\dot{E}x_{termal,Absor}$ and $T_{ave,Abs}$ are the representative of removed thermal exergy from the absorber and average temperature of the absorber, which is calculated by Eq. (73)

$$T_{ave,Abs} = (T_{10} + T_6 + T_1 + T_{18} + T_{19}) / 5 \tag{73}$$

$$Ex_{18} + \dot{E}x_{termal,Abs} = Ex_{19} + \dot{E}x_{Des,Abs} \tag{74}$$

where Ex_{18}, Ex_{19} and $\dot{E}x_{Des,Abs}$ are the representative of the inlet and outlet exergy of exhaust gasses going through the absorber, and exergy destruction rate in absorber, respectively.

For Condenser 2:

Schematic of the condenser 2 has been shown in figure 4.12.

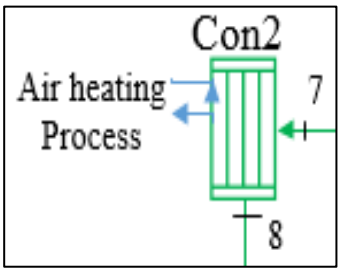

Figure 4.14: Schematic of the condenser 2.

The following equation are used for condenser 2:

Mass balance:

$$\dot{m}_7 = \dot{m}_8 \tag{75}$$

where $\dot{m}_7$ and $\dot{m}_8$ are the inlet and outlet mass flow rate of liquid water going through the condenser 2.

Energy balance:

$$\dot{Q}_{out,Con2} = \dot{m}_7 h_7 - \dot{m}_8 h_8 \tag{76}$$

where h_7 and h_8 are the inlet and outlet enthalpy of liquid water going through the condenser 2. $\dot{Q}_{out,Con2}$ is the removed heat from the condenser.

Exergy analysis:

$$\dot{E}x_{termal,Con2} = \dot{Q}_{Con2}(1 - T_0 / T_{ave,Con2})$$

(77) where, $\dot{E}x_{termal,Con2}$ and $T_{ave,Con2}$ are the representative of removed thermal exergy from the condenser 2 and average temperature of the condenser 2, which is calculated by Eq. (78)

$$T_{ave,Con2} = (T_8 + T_7)/2 \tag{78}$$

$$Ex_7 = Ex_8 + \dot{E}x_{termal,Con2} + \dot{E}x_{Des,Con2} \tag{79}$$

where Ex_7, Ex_8 and $\dot{E}x_{Des,Con2}$ are the representative of the inlet and outlet exergy of liquid water going through the condenser 2, and exergy destruction rate in the condenser, respectively.

For Heat Exchanger 3

Schematic of the heat exchanger 3 has been shown in figure 4.13.

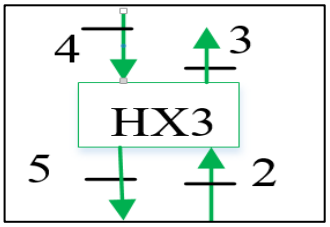

Figure 4.15: Schematic of the heat exchanger 3

The following equations are used for HX3:

Mass balance:

$$\dot{m}_4 = \dot{m}_5 \tag{80}$$

where $\dot{m}_4$ and $\dot{m}_5$ are the inlet and outlet mass flow rate of the solution going through the expansion valve.

Concentration balance:

$$x_5 = x_4$$

(81)

where, X_4 and X_5 are the concentration values of the weak and strong solution going through heat exchanger.

Energy balance:

$$\dot{m}_4 h_4 - \dot{m}_5 h_5 = \dot{m}_3 h_3 - \dot{m}_2 h_2 \tag{82}$$

where h_4 and h_5 are the representative of inlet and outlet enthalpy of the strong solution, h_2 and h_3 are the inlet and outlet enthalpy of the weak solution, going through the heat exchanger 3.

Exergy balance:

$$Ex_2 + Ex_5 = Ex_6 + Ex_3 + Ex_{Des,HX3} \quad (83)$$

where Ex_4 and Ex_5 are the representative of inlet and outlet exergy of the strong solution, Ex_2 and Ex_3 are the inlet and outlet exergy of the weak solution, going through the heat exchanger 3.

For Expansion Valves:

Schematic of the Exv1 and Exv2 has been shown in figure 4.14.

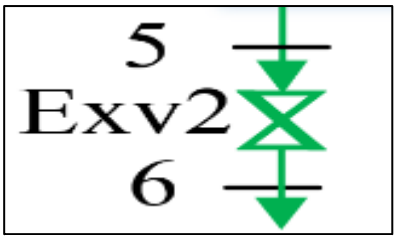

Figure 4.16: Schematic of the expansion valves

The following equations are used for expansion valve:

$$m_4 = m_5 \quad (84)$$

$$x_6 = x_5 \quad (85)$$

$$h_5 = h_6 \quad (86)$$

$$h_9 = h_8 \quad (87)$$

$$Ex_8 + Ex_5 = Ex_6 + Ex_3 + \dot{E}x_{Des,Exv} \tag{88}$$

where h_i, Ex_i, and $\dot{E}x_{Des,Exv}$ are the representative of enthalpy of the state, exergy of the state, and exergy destruction rate of expansion valves, respectively.

For Pump 3

Schematic of the pump 3 has been shown in figure 4.15.

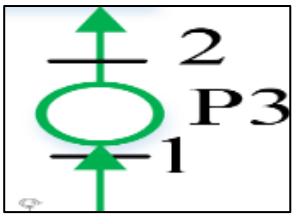

Figure 4.17:
Schematic of the P3

The following equations are used for pump 3:

Mass balance:

$$\dot{m}_2 = \dot{m}_1 \tag{89}$$

where $\dot{m}_1$ and $\dot{m}_2$ are the inlet and outlet mass flow rate of solution going through the pump 3.

Energy analysis:

$$\dot{W}_{P3} = \dot{m}_2 v_2 \left(P_2 - P_1\right) / \eta_{P3} \tag{90}$$

$$\eta_{P3} = \frac{\dot{W}_s}{\dot{W}_a} \tag{91}$$

where, $\dot{W}_{P3}$, P_2, P_1, v_2, and $\eta_{s,P3}$ are the produced power by pump 3, inlet and outlet pressure of the weak solution going through the pump 3, inlet specefic volume liquid weak solution, isentropic efficiency, respectively.

Exergy analysis:

$$\dot{E}x_{Des,P3} + Ex_2 = Ex_3 + \dot{W}_{P3} \quad (92)$$

where Ex_2 and Ex_2 are the representative of inlet and outlet exergy going through the pump 3. $\dot{E}x_{Des,P3}$ is the exergy destruction in pump 2.

For Evaporator

Schematic of the evaporator has been shown in figure 4.16.

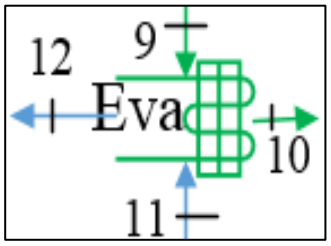

Figure 4.18: Schematic of the Eva

The following equations are used for evaporator:

Energy balance:

$$\dot{m}_9 = \dot{m}_{10} \quad (93)$$

where $\dot{m}_9$ and $\dot{m}_{10}$ are the inlet and outlet mass flow rate of water going through the evaporator.

$$\dot{m}_{11} = \dot{m}_{12}$$

(94)

where, $\dot{m}_{11}$ and $\dot{m}_{12}$ are the inlet and outlet mass flow rate of water going through the evaporator, which considered to transfer the heat to the evaporator.

Energy balance:

$$\dot{Q}_{in,eva} = \dot{m}_9(h_{10} - h_9)$$

(95)

$\dot{Q}_{in,eva}$ is the absorbed heat by evaporator.

Exergy balance:

$$\dot{E}x_{termal,Eva} = \dot{Q}_{in,Eva}(1 - T_0 / T_{ave,Eva}) \quad (96)$$

where, $\dot{E}x_{termal,Eva}$ is the absorbed thermal exergy by evaporator, and $T_{ave,Eva}$ is the average temperature of evaporator, that has been obtained from Eq. (97).

$$T_{ave,Eva} = (T_{10} + T_9)/2 \quad (97)$$

Exergy balance:

$$Ex_9 + Ex_{11} = Ex_{10} + E\,x_{12} + \dot{E}x_{Des,Eva} \quad (98)$$

where Ex_i, $\dot{E}x_{Des,Eva}$ are the representative of exergy flow of the state and exergy destruction rate in the evaporator.

4.1.5 Electrolyzer

Schematic of the electrolyzer has been shown in figure 4.17.

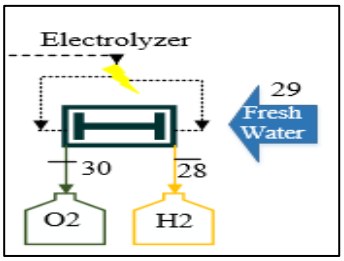

Figure 4.19: Schematic of the electrolyzer

Standard chemical exergy of inlet and outlet of electrolyzer can be calculated by using table 4.2.

$$\dot{m}_{H_2} = (W_{ORC,T}\eta_{Elz}) / HHV_{H_2} \quad (99)$$

HHV_{H_2}, η_{Elz}, and $\dot{m}_{H_2}$ are the high heat value, efficiency of the electrolyzer, and produce hydrogen mass flow rate.

The chemical exergy of H_2, O_2, and H_2O can be obtained from the following equations:

$$Ex_{ch,H_2} = \left(236.09 \times 1000\right) / M_{H_2} \quad (100)$$

$$Ex_{ch,O_2} = \left(3.97 \times 1000\right) / M_{O_2} \quad (101)$$

$$Ex_{ch,H_2O} = \left(0.9 \times 1000\right) / M_{H_2O} \quad (102)$$

where M_{H_2}, M_{O_2}, and M_{H_2O} are the molar mass of H_2, O_2, and H_2O.

Table 3: Standard chemical exergy for O2, H2, and H2O (T= 298.15 K, P = 101.325 kPa) (Szargut, 2007).

Substance	State	Molecular mass(kJ/mol)	Enthalpy of devaluation(kJ/mol)	Standard chemical exergy(kJ/mol)
H_2	g	2.01594	241.818	236.09
H_2O	l	18.01534	-44.012	0.9
O_2	g	31.9988	0	3.97

The physical exergy of H_2, O_2, and H_2O can be obtained from:

$$Ex_{ph,H_2} = \dot{m}_{28}[(h_{28} - h_0) - T_0(s_{28} - s_0)] \quad (103)$$

$$Ex_{ph,O_2} = \dot{m}_{30}[(h_{30} - h_0) - T_0(s_{30} - s_0)] \quad (104)$$

$$Ex_{ph,H_2O} = \dot{m}_{29}[(h_{29} - h_0) - T_0(s_{29} - s_0)] \quad (105)$$

Which, T_0, S_0, and h_0 are the representative of temperature, entropy, and the enthalpy of the ambient condition.

$$\dot{m}_{29}(Ex_{chH_2O} + Ex_{phH_2O}) + \dot{W}_{ORC,T}\,\eta_{Elz} = \dot{m}_{28}(Ex_{chH_2} + Ex_{phH_2}) + \dot{m}_{30}(Ex_{chO_2} + Ex_{phO_2}) + \dot{E}x_{Des,Elz} \quad (106)$$

where, $Ex_{ph,i}, Ex_{ch,i}$, and $\dot{E}x_{Des,Elz}$ are the representative of physical exergy and chemical exergy of the state, exergy destruction rate and inlet heat of electrolyzer, respectively.

For Air Conditioner:

Schematic of the air conditioner (AC) has been shown in figure 4.18.

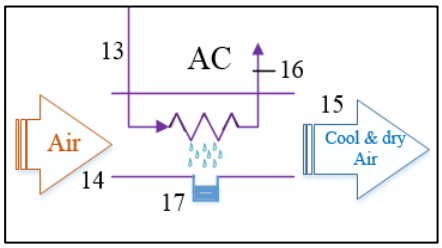

Figure 4.20: Schematic of the AC

The following equation are used for air conditioner system:

Mass balance:

$$\dot{m}_{14} = \dot{m}_{15} + \dot{m}_{17} \tag{107}$$

$$\dot{m}_{14} \times \omega_{14} = \dot{m}_{15} \times \omega_{15} + \dot{m}_{moisture(17)} \tag{108}$$

where, $\dot{m}_{14}$ and $\dot{m}_{15}$ are the inlet and outlet mass flow rate of air going through the AC. $\dot{m}_{17}$ is the mass flow rate of moisture. ω_{14} and ω_{15} are the relative humidity of the inlet and outlet air going through the AC.

Energy balance:

$$\dot{Q}_{out,AC} = \dot{m}_{16} \times \left(h_{16} - h_{13}\right) \tag{109}$$

$$\dot{m}_{14} h_{14} = \dot{m}_{17} h_{17} + \dot{m}_{15} h_{15} + \dot{Q}_{out,AC} \tag{110}$$

where, h_{14} and h_{15} are the inlet and outlet enthalpy of air going through the AC. h_{17} is the enthalpy of moisture. $\dot{Q}_{out,AC}$ is the removed heat from the air in AC.

Exergy balance:

$$\dot{E}x_{termal,AC} = \left(1 - T_0 / T_{avg}\right) \times \dot{Q}_{out,AC} \tag{111}$$

$$\eta_{AC} = \left(\frac{\dot{m}_{air,15} h_{15}}{\dot{Q}_{AC}} \right) \tag{112}$$

where Ex_i, $\dot{E}x_{Des,AC}$, and η_{AC} are the representative of exergy of the state, exergy destruction rate, thermal efficiency of AC and rejected heat of AC, respectively.

4.2 Efficiency

The energy efficiency is defined as the proportion of effective energy generated (such as electricity, hydrogen, etc.), to the consumed fuel supplied to the multi-generation power plant. For modeling of the multi-objective system, we consider additive energy efficiencies, which includes all of the production of the system.

For SEACS unit the energetic and exergetic coefficient of performance (COP_{en} and COP_{ex}) are defined by:

$$COP_{en} = \frac{\dot{Q}_{Cooling} + \dot{Q}_{out,Con2}}{\dot{Q}_{in,Gen} + \dot{W}_{P3}} \tag{113}$$

$$COP_{ex} = \frac{\dot{E}x_{termal,Cooling} + \dot{E}x_{termal,Con2}}{\dot{E}x_{termal,Gen} + \dot{W}_{P3}}$$

(114)

The produced electricity (net power) of the system can be obtained from Eq. (115)

$$Electricity = \dot{W}_{net} = \dot{W}_{LPT} + \dot{W}_{HPT} - (\dot{W}_{P1} + \dot{W}_{P2} + \dot{W}_{P3}) \tag{115}$$

The produced heating of the system can be obtained by Eq. (116).

$$\dot{Q}_{heating} = \dot{Q}_{out,Con2} + \dot{Q}_{out,Con1} + \dot{Q}_{out,abs} \tag{116}$$

$$\dot{E}x_{termal,heating} = \dot{E}x_{termal,Abs} + \dot{E}x_{termal,Con1} + \dot{E}x_{termal,Con2} \tag{117}$$

The produced cooling of the system can be obtained by following equations:

$$\dot{Q}_{Cooling} = \dot{m}_{11}(h_{11} - h_{40}) \tag{118}$$

$$\dot{E}x_{termal,Cooling} = \dot{Q}_{Cooling}(1 - T_0 / T_{ave,Eva}) \tag{119}$$

The exergetic efficiency (ψ_{MG}) and overall utilization factor (ε_{MG}), can be obtained by following equations:

$$\varepsilon_{MG} = \frac{\dot{W}_{net} + \dot{Q}_{heating} + \dot{m}_{H_2} LHV_{H_2} + \dot{Q}_{Cooling} + \dot{m}_{15} h_{15}}{\dot{m}_{Biomass} LHV_{Biomass}} \tag{120}$$

$$\psi_{MG} = \frac{\dot{W}_{net} + \dot{E}x_{termal,heating} + \dot{m}_{H_2} LHV_{H_2} + \dot{E}x_{termal,Cooling} + \dot{m}_{15} \dot{E}x_{15}}{\dot{m}_{Biomass} \dot{E}x_{Biomass}} \tag{121}$$

where $\dot{E}x_{Biomass}$ is the exergy of biomass, and it is defined by (Bingöl, 2011):

$$\dot{E}x_{biomass} = \rho LHV_{moisture} \tag{122}$$

$$\rho = \frac{1.0414 + 0.0177(\frac{H}{C}) - 0.3328(\frac{O}{C})\{1 + 0.0537(\frac{H}{C})\}}{1 - 0.4021(\frac{O}{C})} \tag{123}$$

4.3 Specific CO_2 Emissions and Sustainability Analysis

For studying the GHGs emissions of the multi-generation plant, the CO_2 emissions are calculated for the whole of the plant. The specific CO_2 emissions can be defined as (Cohce, 2011):

$$\alpha_{MG} = \frac{\dot{m}_{CO_2}}{\dot{W}_{net} + \dot{Q}_{heating} + \dot{m}_{H_2} LHV_{H_2} + \dot{Q}_{Cooling} + \dot{m}_{15} h_{15}} \tag{124}$$

Sustainable energy resources consumption and operation of non-renewable resources fuel in high efficient condition are the indispensable notes to improve environmental sustainability. A sustainability index (SI) is applied (Dincer, 2012):

$$SI=1/D_P \tag{125}$$

In which DP is the depletion number, defined as the proportion of exergy destruction to used exergy:

$$D_P=Ex_{des,total}/Ex_{total}$$

According to (148) as exergy destruction of system decreases, environmental impacts decreases too. Furthermore, the sustainability index shows how the exergy efficiencies influence the sustainable development:

$$SI=\frac{1}{1-\psi} \tag{126}$$

where ψ is the exergy efficiency.

Chapter 5

RESULTS AND DISCUSSION

In this chapter, we discussed about multi-generation model, and also its parameters such as enthalpies, environmental effects, irreversibility, energy and exergy efficiencies of the work.

5.1 Modeling Parameters and Results Summary

Table 3 lists the thermo-physical properties of the modeled utility. The variation of these parameters affect the performance of the cycles.

Table 4: Input data applied in simulate the system.

Parameter	Value	Parameter	Value	Parameter	Value
Ambient temperature (K)	293.15	LPT inlet pressure(kPa)	3900	SEACS strong solution concentration (%)	56.94
Biomass mass flow rate ($kg.s^{-1}$)	0.125	LPT inlet mass flow rate ($kg.s^{-1}$)	0.36	SEACS weak solution concentration (%)	52.25
HPT inlet pressure (kPa)	12500	ORC,T inlet pressure (kPa)	589.8	Generator temperature (K)	397
HPT inlet mass flow rate ($kg.s^{-1}$)	0.36	ORC pump inlet mass flow rate ($kg.s^{-1}$)	0.63	Generator pressure ($kg.s^{-1}$)	4.81
PEM electrolyzer temperature (K)	298.15	Evaporator temperature (K)	280.2	AC temperature (K)	286.2
ORC pump inlet temperature (K)	300	Evaporator pressure ($kg.s^{-1}$)	1	AC pressure ($kg.s^{-1}$)	100

Some thermodynamic specifications are chosen as output data through the simulation process based on thermodynamical modeling. These data are presented in Table 5.

Table 5: Parameter values from the energetic and exergetic analyses of the system.

Parameter (Unit)	Value
Biomass flow rate, $\dot{m}_{biomass}$ ($kg.s^{-1}$)	0.125
Heating load, $\dot{Q}_{heating}$ (kW)	1332
Cooling load, $\dot{Q}_{Cooling}$ (kW)	223.8
Electricity, $\dot{W}_{net}$ (kW)	372.8
Overall utilization factor	2.096
Exergy efficiency, ψ_{MG} (%)	24.03
COP_{en} of SEACS (-)	0.8177
COP_{ex} of SEACS (-)	0.2916
ORC mass flow rate, $\dot{m}_{ORC}$ ($kg.s^{-1}$)	0.63
produced power by ORC,T (kW)	11.55
Hydrogen production mass flow rate, $\dot{m}_{Hydrogen}$ ($kg.hr^{-1}$)	0.1642
Hot water mass flow rate, $\dot{m}_{HW}$ ($kg.s^{-1}$)	10.727
Conditioned air mass flow rate, $\dot{m}_{AC}$ ($kg.s^{-1}$)	0.1
Specific CO_2 emission, ε_{MG} ($kg.MWh^{-1}$)	0.3538
Sustainability Index	1.316
Power to heating ratio (-)	0.3522
Power to cooling ratio (-)	2.091
Total exergy destruction rate (kW)	1457

5.2 Exergy Analyses

The study, method, and assessments that was explained earlier are applied to evaluate the results, which contain CO_2 emissions, exergy efficiency and irreversibility rate of the components. Then parametric study of these results are studied based on varying the ambient temperature, the boilers outlet temperature, and the biofuel mass flow rate. The exergy assessment outcomes are tabulated in figure 5.1. As seen in the figure, the maximum exergy destruction occurs in the CC. The prime cause of this high irreversibility depends on the combustion of the fuel. The difference between the inlet and outlet temperature of CC is the second important reason of irreversibility in the chamber. Since the boiler of RSRC unit (boiler 1) has a very high-temperature superheated steam at the outlet, the second largest irreversibility comes from that equipment.

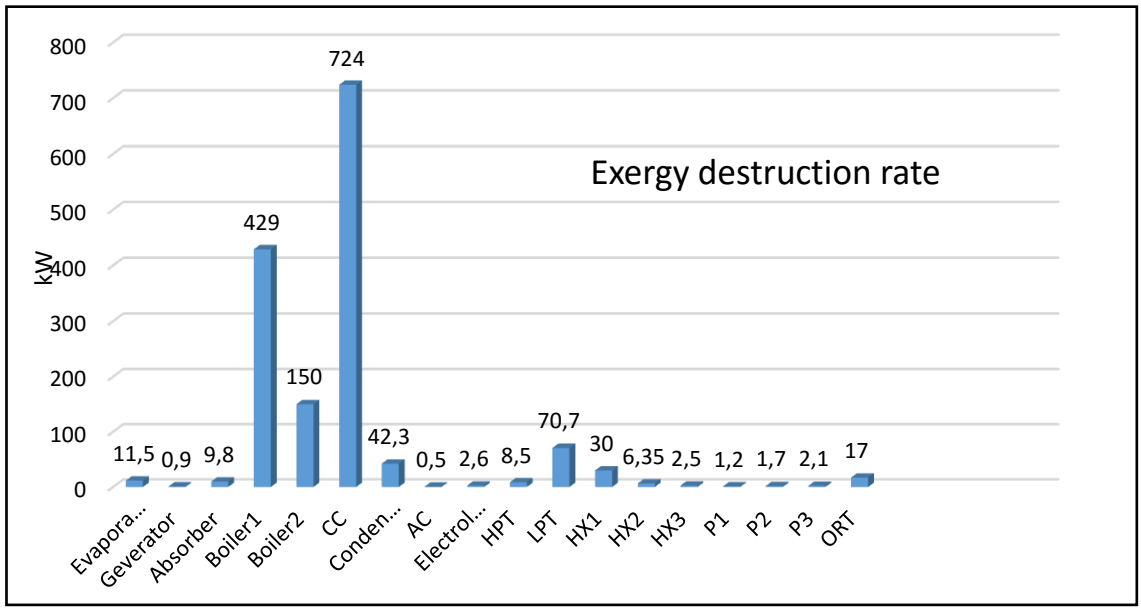

Figure 5.1: Exergy destructions of the components

Figure 5.2 shows the dimensionless exergy destruction in each component. These portions are helpful to prioritizing exergy irreversibility.

The dimensionless exergy destruction in CC is greater than other equipment. Hence, in order to develop the exergy conversation, the combustion process would be an important part to pay attention and study. Moreover, figure 5.2 illustrates that the both boilers expose significant irreversibility, because they directly utilize hot exhaust gasses, for evaporation process.

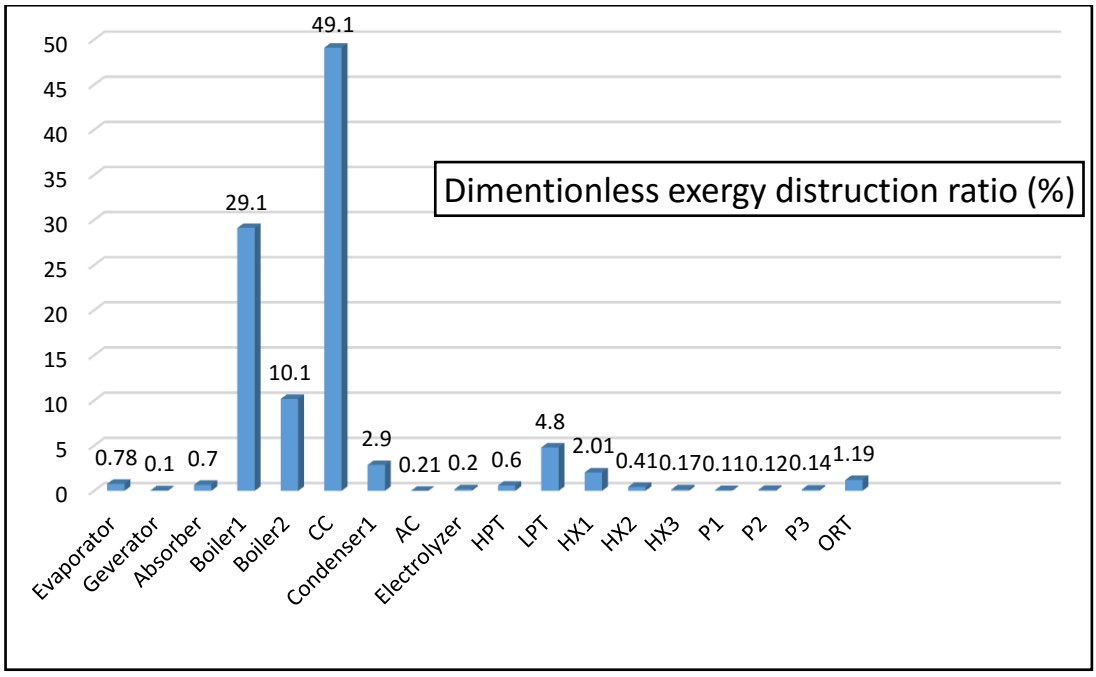

Figure 5.2: Dimensionless exergy destructions of components.

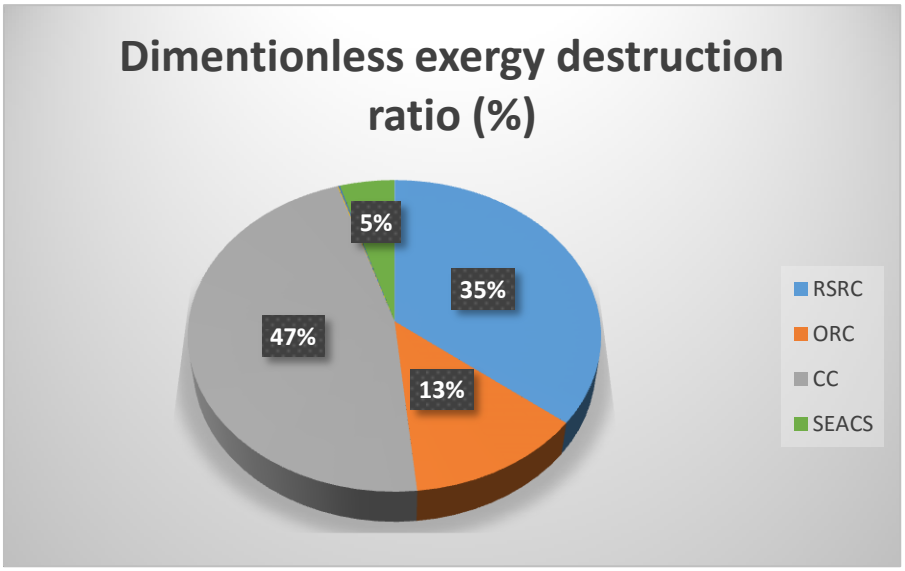

Figure 5.3: Dimensionless exergy destructions ratio of cycles.

The exergy destruction of all units is shown in figure 5.3. It shows that the highest exergy destruction belongs to the combustion process and RSRC unit.

5.3 Parametric Study

The effect of change in some factors on the thermodynamical proficiency of the multi-generation is assessed. Since the biofuel mass flow rate, the boilers exhaust gas temperature, and the ambient temperature significantly affect the performance of the system (e.g., energy and exergy efficiencies), they are major considered parameters in this discussion.

5.3.1 Effect of Ambient Temperature on Exergy Performance

Ambient temperature is one of the crucial parameters that affects both exergy efficiency and exergy destruction. Figure 5.4 shows the effect of varying ambient temperature on the plant and how it affect the overall exergy efficiencies and total exergy destruction ratio. By raising the ambient temperature from 281 K to 337 K, there is a downward trend for exergetic efficiency and upward trend for total destruction ratio. By increasing ambient temperature, exergetic efficiency decline

from 26.21% to 16.08%. In addition, one can say the total exergy destruction ratio increases from 1439 kW to 1602 kW.

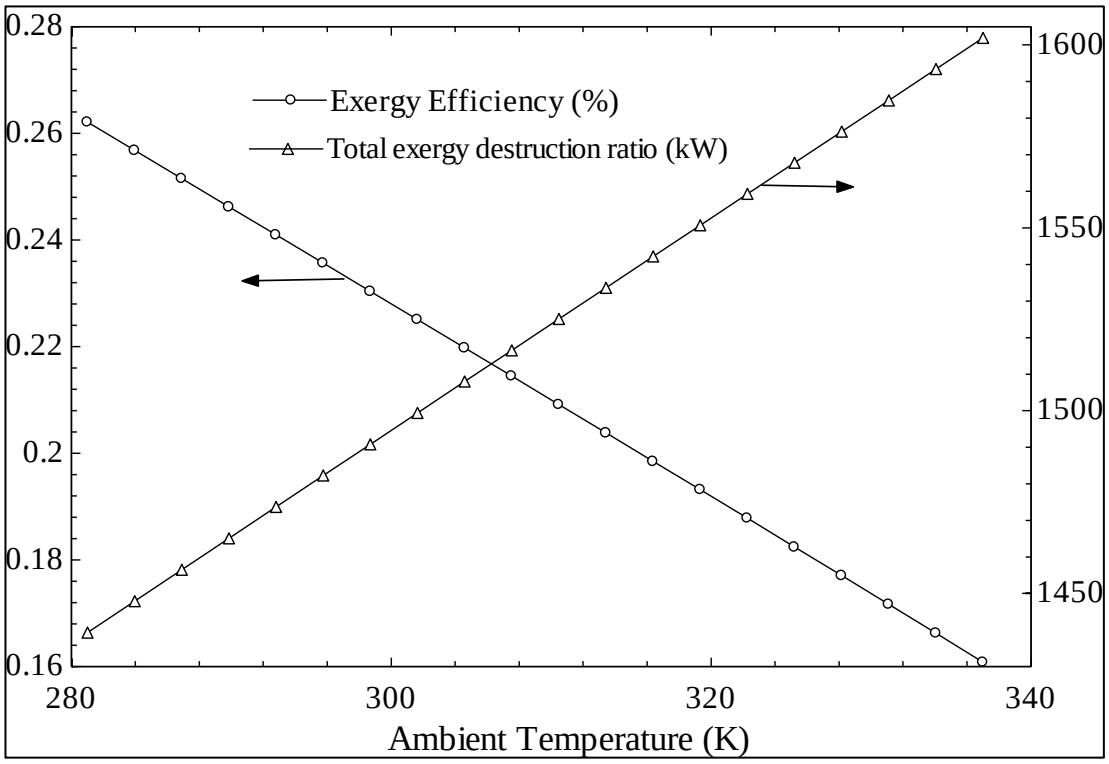

Figure 5.4: Effect of ambient temperature on total exergy destruction rate and exergy efficiency.

The effect of ambient temperature on exergy destructions has been investigated more comprehensively in the following section. Figure 5.5 shows the effect of varying ambient temperature and its effect on exergy destruction of the main equipment. As seen in the figures, while the ambient temperature increased, the irreversibility of CC and boiler 1 will increases and also it's worth mentioning that these two components play a significant role in total irreversibility of the system.

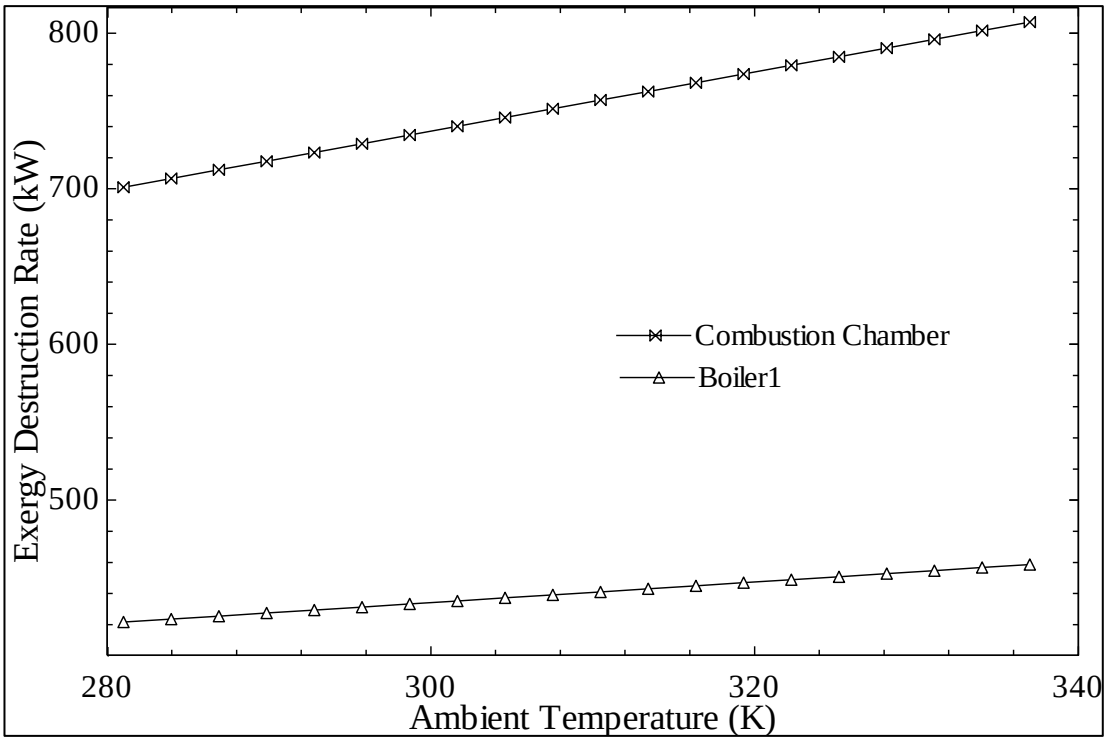

Figure 5.5: Effect of ambient temperature on exergy destruction of main equipment (CC and boiler 1)

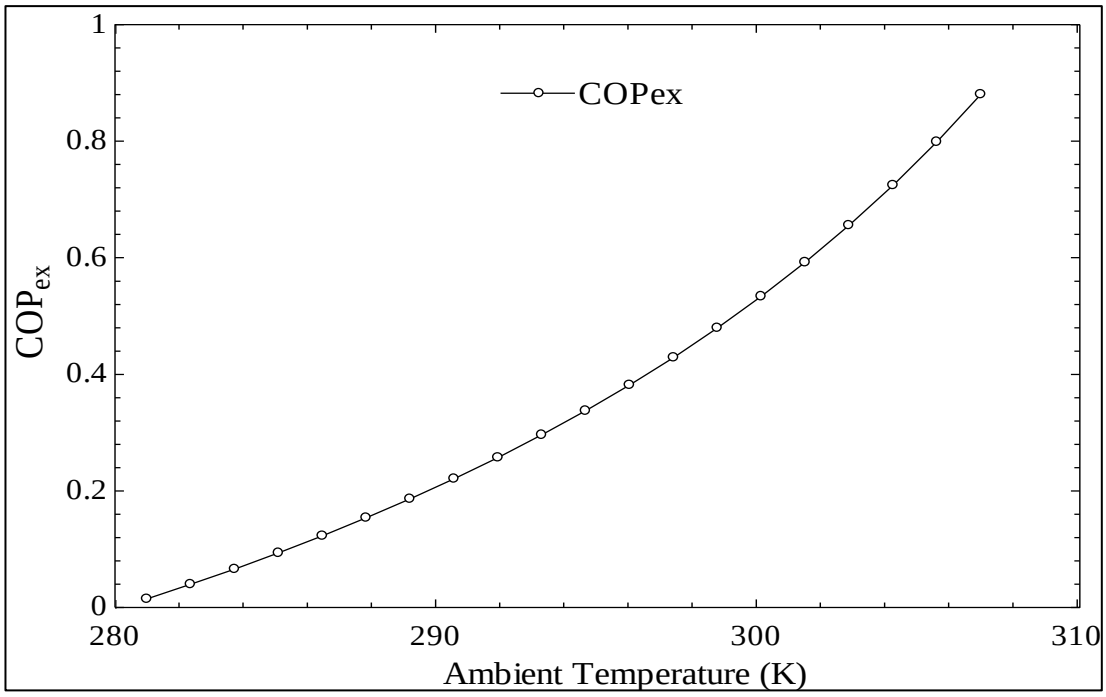

Figure 5.6: Effect of ambient temperature on COPex

The effect of ambient temperature on the exergetic coefficient of performance (COP_{ex}), for SEACS is shown in Figure 5.6. It is seen that an increase in ambient temperature has a positive effect on COP_{ex}. While the ambient temperature increases from 281 K to 307 K the COP_{ex} rises from 0.15 to 0.83. The increase of absorbed exergy by evaporator are the main reason for COP_{ex} improvement.

5.3.2 Effect of Biofuel Mass Flow Rate.

The effects of biofuel mass flow rate on the production rate are shown in Figure 5.7. It is understandable that with more biofuel consumption, the flame will get larger, therefore the amount injected heat to the system will surge. In addition, the analyses show that any increase in the biofuel (from 0.125 kg/h to 0.22 kg/h), leads to an increase in received heat by the boilers and the generator. Therefore, the produced power by all three turbines increases (by HPT from 3.793 kW to 379.8 kW, by LPT from 348 kW to 704.1 kW and by ORC turbine from 111.3 kW to 486.7 kW). These trends result in more electricity and hydrogen. Moreover, injected heat to the

generator increases from 269.9 kW to 482.8 kW, and as the weak LiBr-Water solution of the generator receives more heat, more water evaporates. Consequently, the cooling in the evaporator increases.

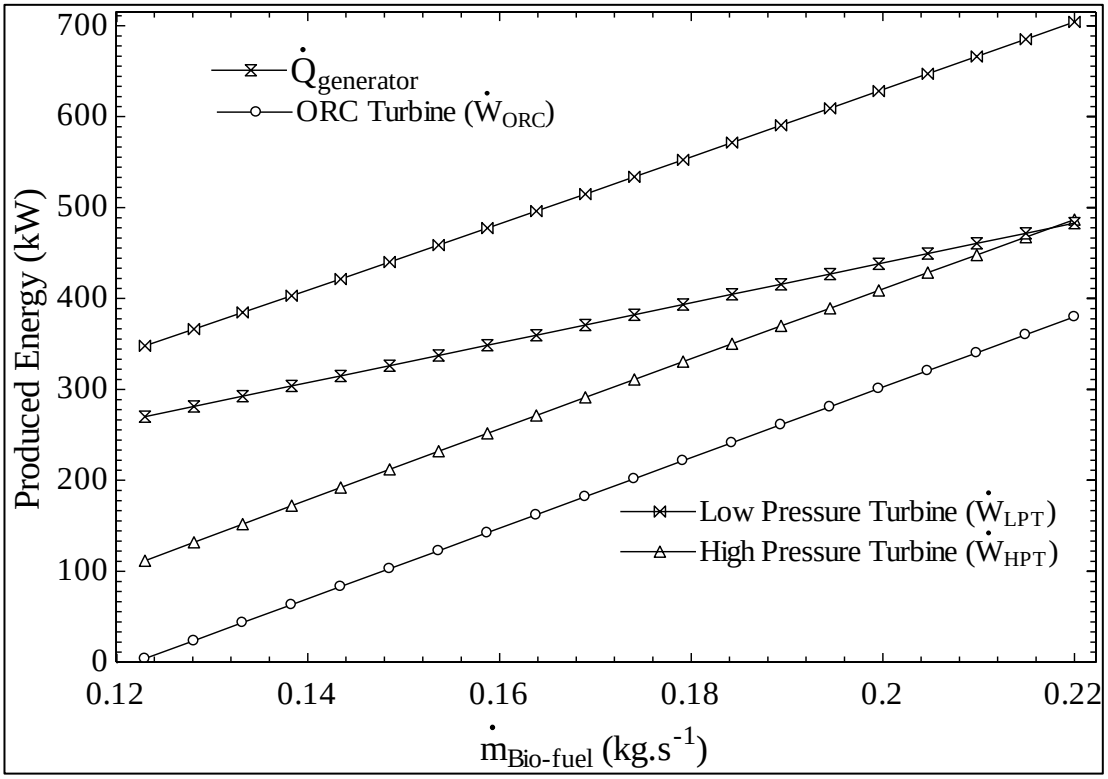

Figure 5.7: Effects of biofuel mass flow rate on productions.

Effects of biofuel mass flow rate on exergy destruction of the main components have been shown in figure 5.8. As expected due to the extreme boost in transferred thermal exergy, the irreversibility increased in all of the components. By comparing these three equipment (CC, boiler 1, and boiler 2), it is clear that increase in exergy destruction rate in CC is more than boiler 1, and in boiler 1 is more than boiler 2. Since the difference between the inlet fuel temperature and exhaust gasses temperature is high, entropy generation of CC is high as well.

Moreover, the reduction of exhaust gas temperature, which is, occurred in the outlet of boiler 1, and boiler 2. This is the other reason of exergy destruction increment in boiler 1, and boiler 2.

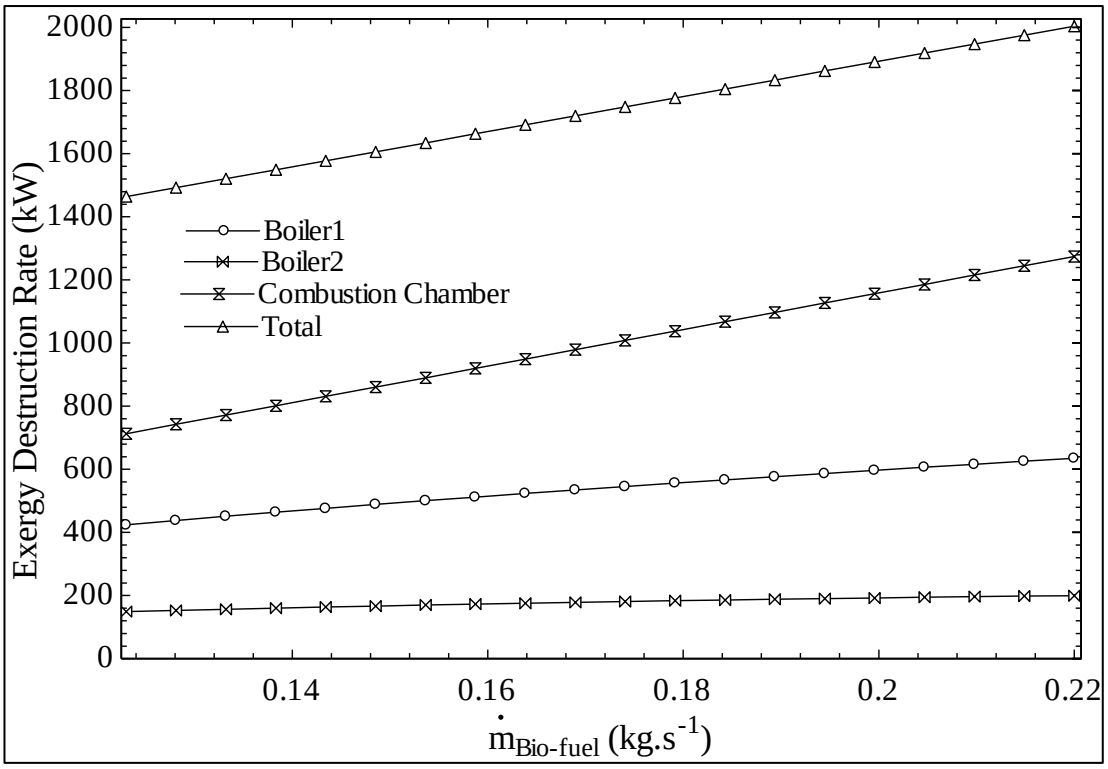

Figure 5.8: Effect of biofuel mass flow rate on the irreversibilities of the main equipment.

Effects of biofuel mass flow rate on the energetic and exergetic efficiency of the multi-generation system have shown in figure 5.9. Any increase in fuel mass flow rate, raises the produced exergy of the system, this positive effect overcomes the negative effect of inflation of exergy destruction. Hence overall exergy efficiency increased from 23.61 % to 35.14 %. Instead, the overall utilization factor did not vary positively, and it declined from 2.11 to 1.731. It means enthalpy losses increases with increase in fuel mass flow rate.

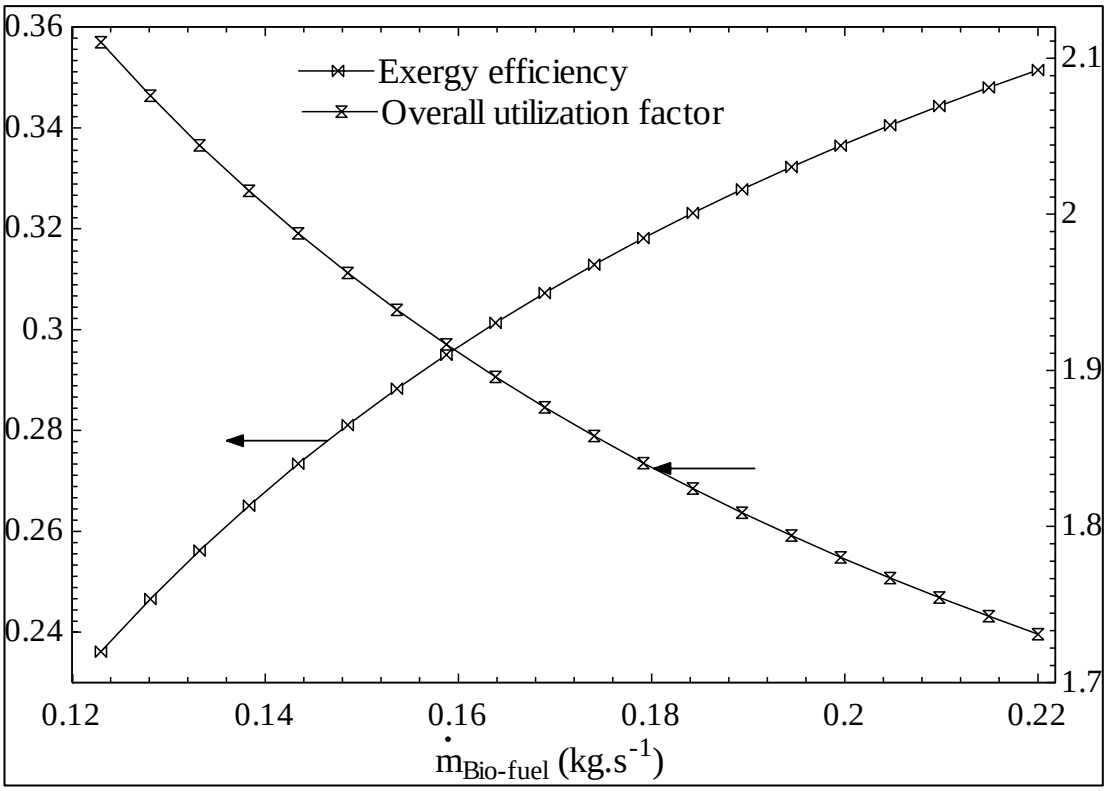

Figure 5.9: Effect of biofuel mass flow rate on the energetic and exergetic efficiency of the multi-generation system.

Environmental impact assessments are applied and compositions of the exhaust gasses of burning biomass fuel, which is pine sawdust, has been analyzed. Figure 5.10 represents the effect of biofuel mass flow rate on carbon dioxide emissions, and on hydrogen production by electrolyzer. It is clear that by supplying more fuel, more heat is injected to boiler 2 so more electricity is generated by ORC turbine (also see figure 5.6 and figure 5.7). Hence, electrolyzer is nourished more by ORC turbine and produce more hydrogen. In figure 5.9 hydrogen production is increased from 0.539 kg/hour to 5.4 kg/hour which effected by increase in fuel mass flow rate from 0.123 kg/s to 0.22 kg/s. Moreover, figure. 5.9 shows the upward trend for carbon dioxide emission that is from 0.1939 kg/s to 0.3521 kg/s.

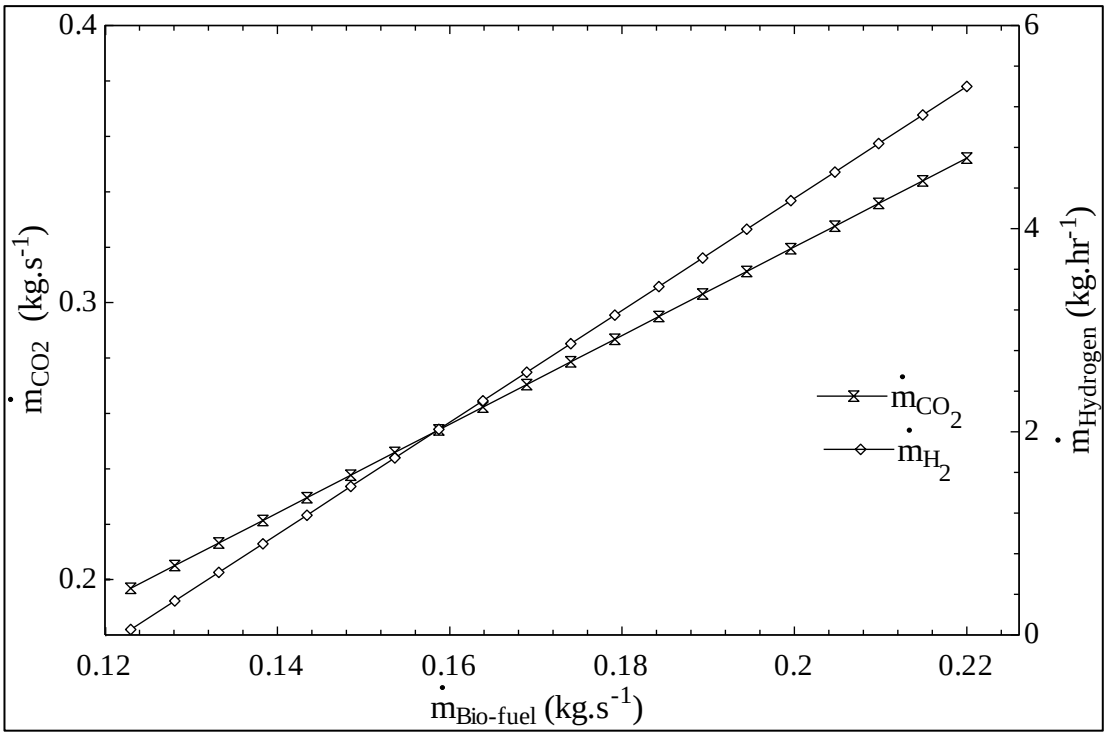

Figure 5.10: Effect of biofuel mass flow rate on the hydrogen production and carbon dioxide emission.

In the modeling process the overall utilization factor, the exergy efficiency, and the CO_2 emission are very important factors. Figure 5.11 represents the results of varying biofuel mass flow rate on CO_2 emission ($\dot{m}_{CO_2}$), overall utilyzation factor (ε_{MG}), and exergy efficiency(ψ_{MG}) of the system, simulstantly. This parametric study (Figure 5.11) helps to analys and describe the relation of these three factors.

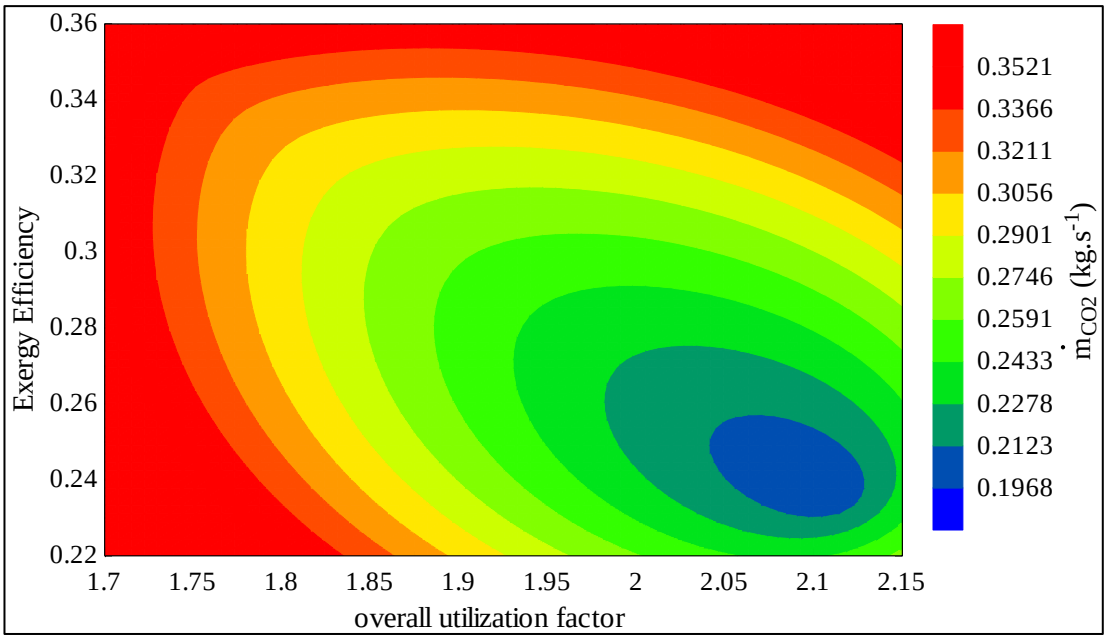

Figure 5.11: Effect of biofuel mass flow rate on the overall utilization factor, exergy efficiency, and CO_2 emissions.

5.3.3 Effect of RSRC Boiler Outlet Temperature

Figure 5.12 shows the effect of boiler 1 exhaust gas temperature on the produced power by HPT, LPT, and ORC turbines. It is observed that an increase in boiler 1 outlet temperature (T_{25}) results in a decrease in RSRC turbines shaft power (LPT and HPT) and increase in ORC turbine shaft power. While boiler 1 outlet temperature increases, boiler 1 absorbs less heat, and more heat is injected to the second boiler (boiler 2), so the ORC turbine inlet temperature increases (based on the mass balance for a control volume around boiler 2). Consequently, more power is produced by ORC turbine (from 0.58 kW to 200.7 kW) and the hydrogen production grows (from 8.2 g/hour to 2.854 kg/hour (also see figure 5.13)). Besides, because of enthalpy drop in inlet flow of LPT (T_{43}) and HPT (T_{41}) produced power declines from 360.2 kW to 267.8 kW and from 125.1 kW to 17.38 kW, respectively.

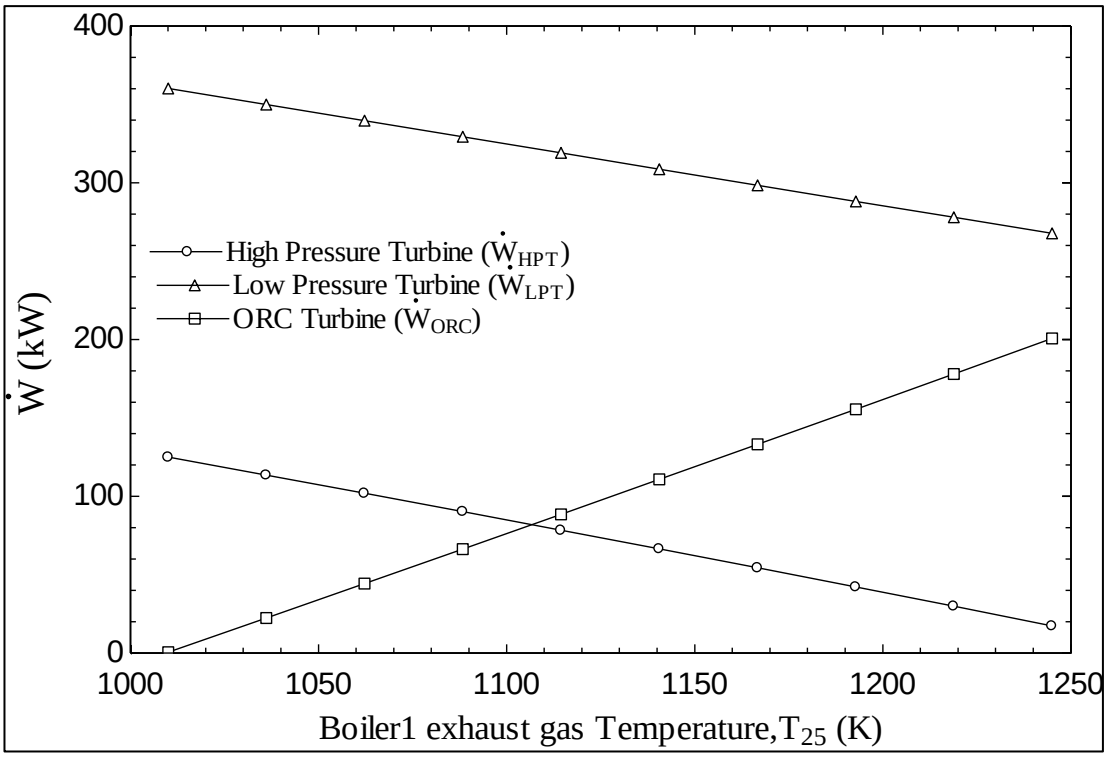

Figure 5.12: Effect of boiler 1 exhaust gas temperature on the produced work by HPT, LPT, and ORC turbine.

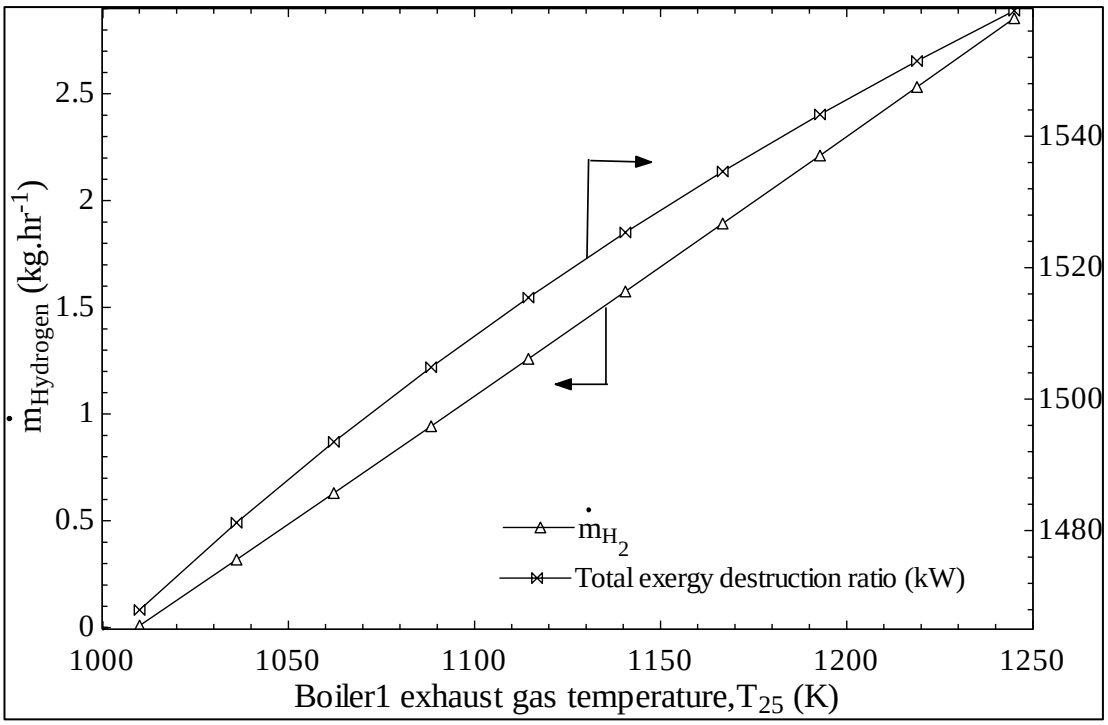

Figure 5.13: Effect of the boiler 1 exhaust gas temperature on the produced hydrogen in electrolyzer and the total exergy destruction ratio.

In addition, the effect of the boiler 1 exhaust gas temperature on the exergy destruction and hydrogen production is illustrated in figure 5.13. It represent that

while the boiler 1 exhaust gasses temperature increased from 1010 K to 1245 K the total exergy destruction of system increased from 1468 kW to 1559 kW. The most important reason of this trend relates to the increase of exergy destruction in boiler 2 and ORC turbine, which presented in figure 5.14. An increase in boiler 1 exhaust gasses temperature, raises produced power by ORC turbine and also hydrogen production (from 8.2 g/hour to 2.854 kg/hour).

Figure 5.14 shows the effect of boiler 1 exhaust gas temperature (T_{25}) on the exergy destruction ratio in boilers. It is observed that an increase in T_{25} results in an increase in boiler 2 exergy destruction rate and a decrease in boiler 1 exergy destruction rate.

It can be concluded that, increase in exergy destruction in boiler 2 is more than the decrease in exergy destruction in boiler 1.

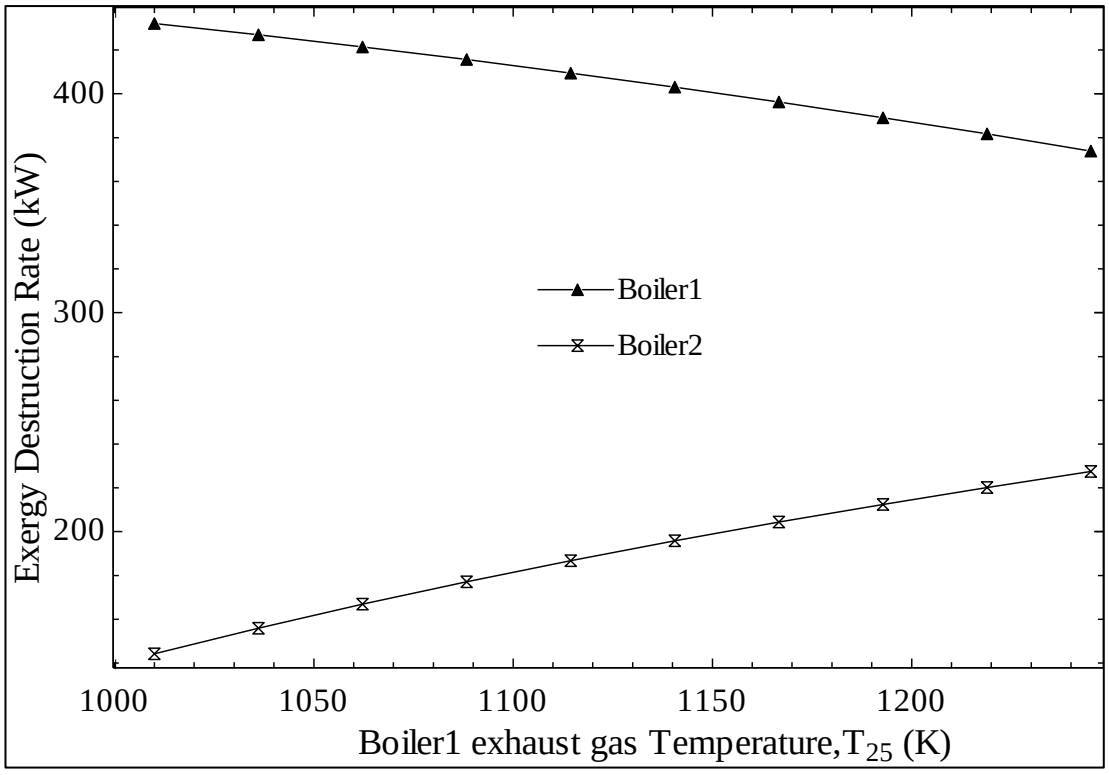

Figure 5.14: Effect of boiler 1 exhaust gas temperature on the produced hydrogen production in electrolyzer and total exergy destruction ratio.

The effect of boiler 1 exhaust gas temperature on overall utilization factor and exergy efficiency has shown in figure 5.15. It has seen that an increase in boiler 2 exhaust gas temperature has a negative effect on both overall utilization factor and exergy efficiency. According to the energy balance for the boiler 1, while boiler 1 exhaust gas temperature increases, the enthalpy of inlet flow to RSRC turbines (LPT and HPT) decreases. This reduction of enthalpy leads to a decrement in produced power by RSRC turbines. Since the generated electricity decreases, therefore the overall utilization factor and the exergy efficiency reduce. Increment in ORC turbine work, is the only positive effect of boosting the temperature (T_{25}), and this advantage is not able to overcome the negative effect on RSRC productions. So that by increase in boiler 1 exhaust gasses temperature from 1010 K to 1245 K the overall utilization factor and exergy efficiency decline from 2.107 to 1.917, and from 0.2447 % to 0.1647 % respectively.

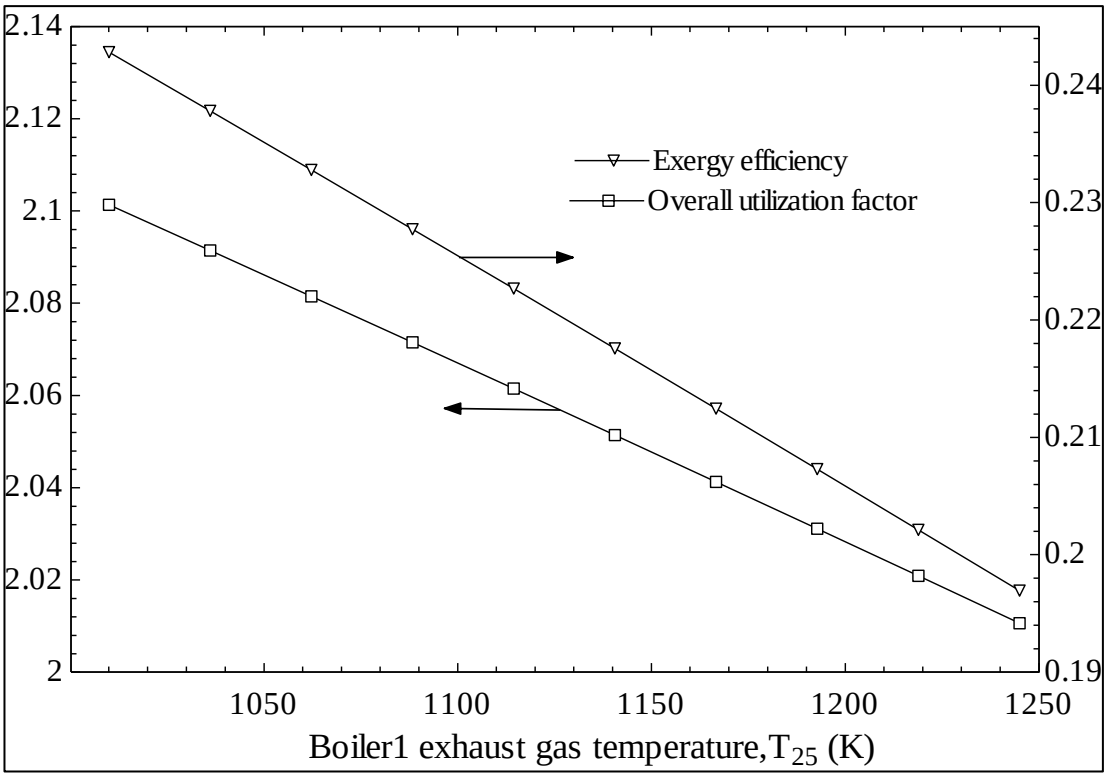

Figure 5.15: Effect of boiler 1 exhaust gas temperature on the overall utilization factor and exergy efficiency.

5.3.4 Effect ORC Boiler Outlet Temperature

The effect of boiler 2 exhaust gas temperature (T_{26} in figure. 3.2), on hydrogen production and injected heat to the generator, are shown in figure 5.16. As seen an increase in boiler 2 exhaust gasses temperature, results an increase in the injected heat to the generator (from 253.8 kW to 288.6 kW), which evaporate more water at state 7 (see figure 3.2). Consequently more water cause more cooling in the evaporator (see figure 4.18).

Moreover, an increase in boiler 2 exhaust gasses temperature, results in an enthalpy drop of ORC turbine inlet flow (h_{35} see figure 3.2), therefore produced work by ORC turbine and hydrogen production decrease. Therefore, by increasing T_{26} from 374 K to 413 K the hydrogen production declines from 0.3975 kg/hour to 1.483 g/hour.

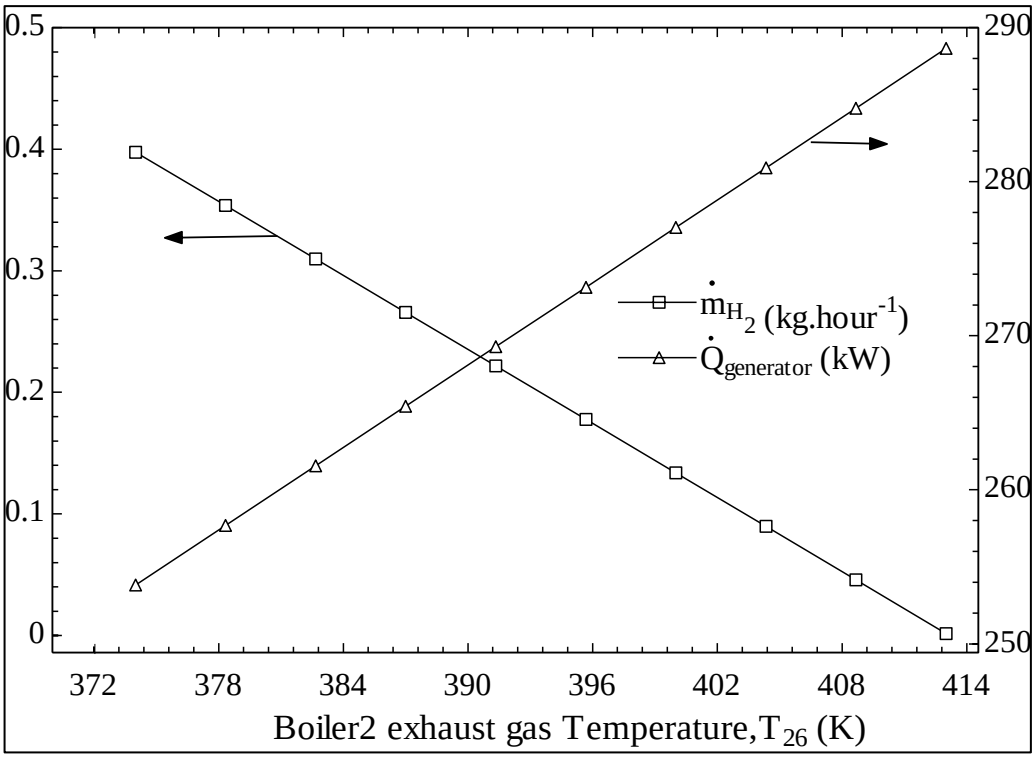

Figure 5.16: Effect of boiler 2 exhaust gas temperature on the overall utilization factor and exergy efficiency.

Figure 5.17 shows the effect of boiler 2 exhaust gasses temperature on utilization factor and exergy efficiency. As seen, by increasing in boiler 2 exhaust gasses temperature from 374K to 413 K, overall utilization factor and exergy efficiency plummet from 2.106 to 2.09 and 24.35 % to 23.8 %.

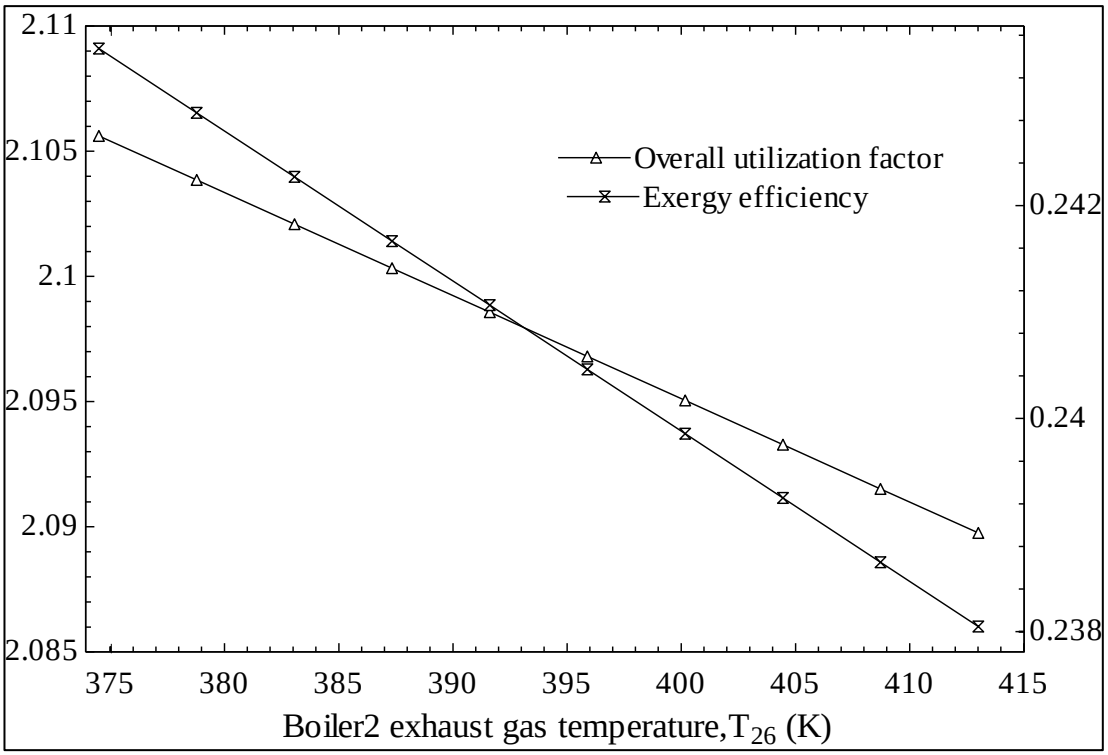

Figure 5.17: Effect of boiler 2 exhaust gas temperature on the overall utilization factor and exergy efficiency.

5.3.5 Effect of Injected Heat to the Generator on SEACS Performance

Any variation in injected heat amount to the generator in SEACS, affects the performance of cooling and dehumidifying units. It was illustrated in sections 5.3.2, 5.3.3, and 5.3.4 an increase in fuel mass flow rate, and boilers exhaust gasses temperature, raised the injected heat to the generator. Effect of injected heat to the generator ($Q_{in,\ Gen}$) on the energetic and exergetic coefficient of performance has shown in figure 5.18. It is clear that an increase in the injected heat to the generator from 277.4 kW to 518.4 kW, results in an increase until critical point then a decrease for both coefficients of performance.

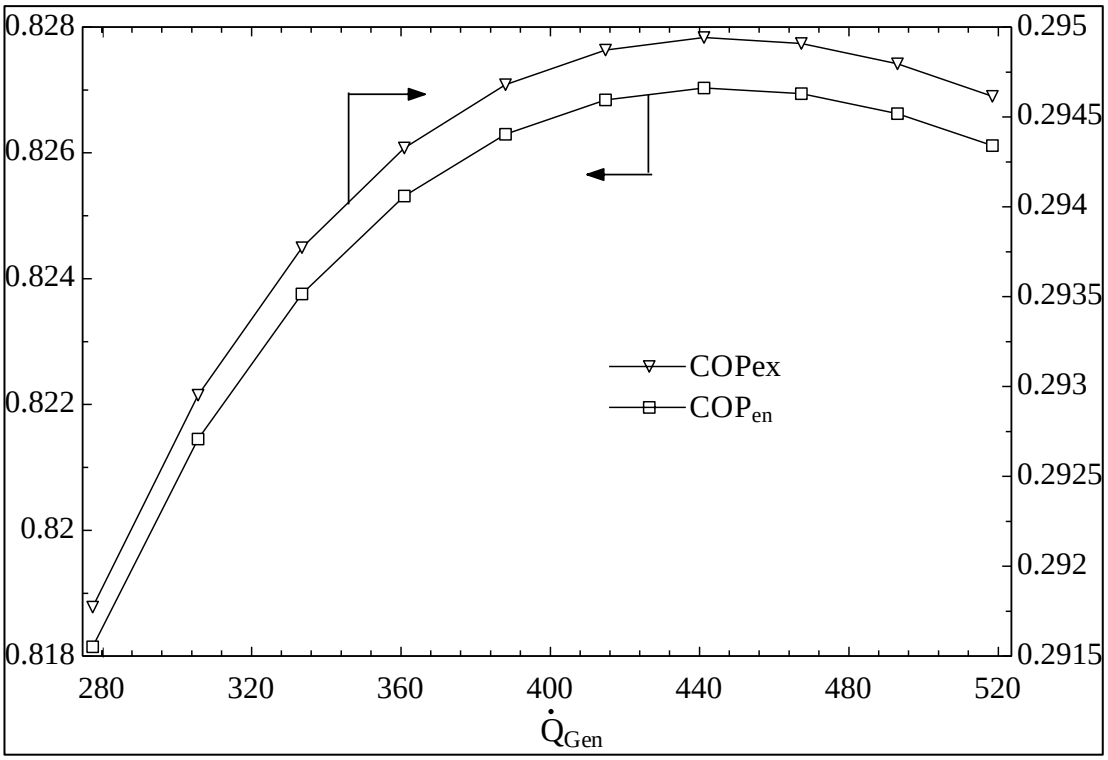

Figure 5.18: Effect of injected heat to the SEACS generator on COP_{ex} and COP_{en}.

5.3.6 Environmental Impact Assessment

The effect of biofuel mass flow rate on specific CO_2 emissions and sustainability index is shown in figure 5.18. By consumption of more biofuel, the specific CO_2 emission rises for multi-generation system. This trend shows that rate of increase in CO_2 production are greater than the rate of increase in useful energy production. However, since exergy efficiency increases (also see figure 5.9), the sustainability index has improved, which is significantly important in multi-objective design.

Variation of environmental impact with boilers exhaust gasses temperature is represented in figure 5.19 and figure 5.20. In both of these figures, it is observed that an increase in boilers exhaust gasses temperature affects the both environmental factors negatively. Therefore, in figure 5.20 and figure 5.21 specific CO_2 emissions has an upward trend, and sustainability has downward trend. Thus, figure 5.20 and

figure 5.21 expresses that according to sustainability issues, the exhaust of boilers should be kept in low temperature.

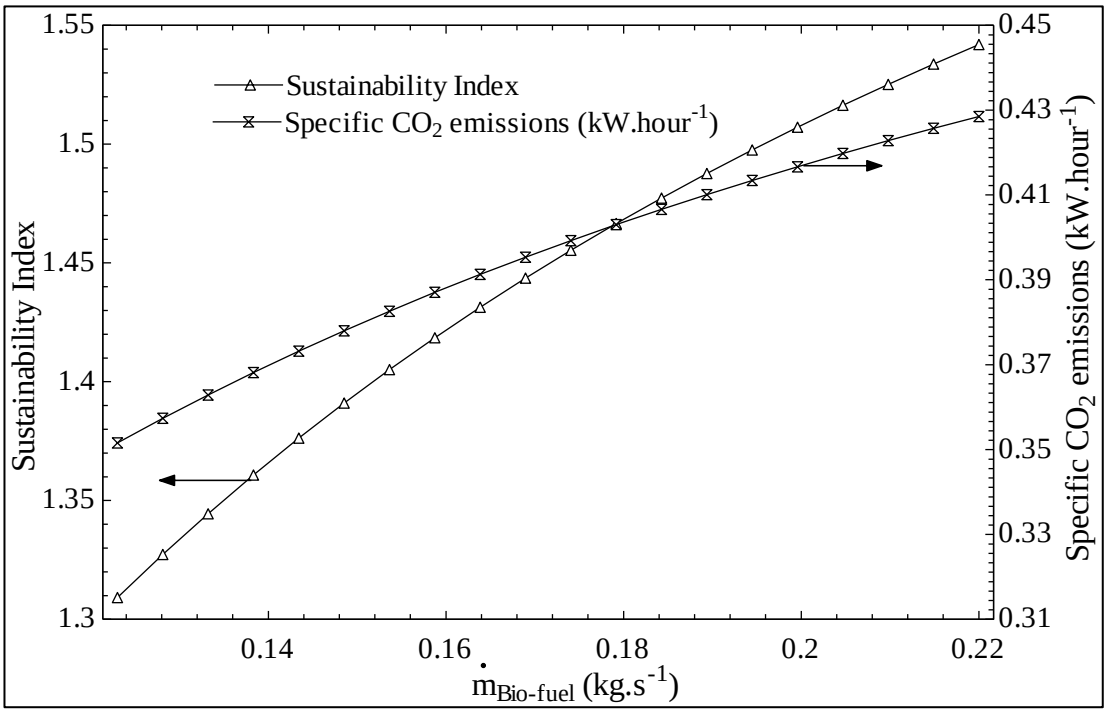

Figure 5.19: Effect of biofuel mass flow rate on the specific CO_2 emissions and sustainability index.

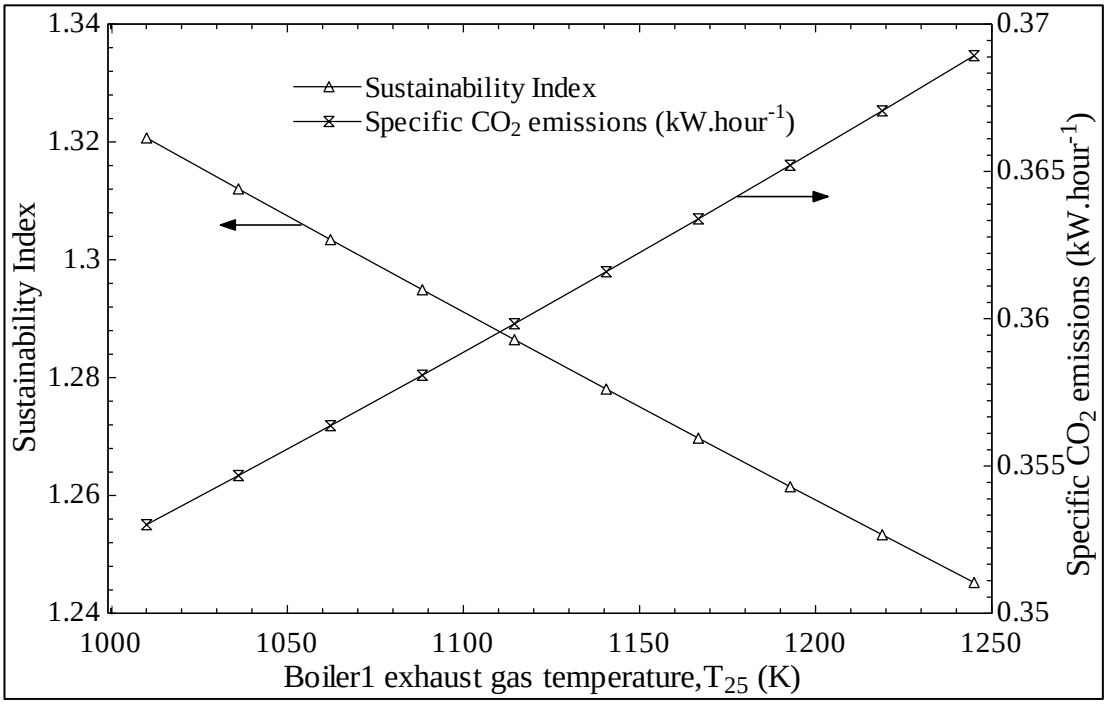

Figure 5.20: Effect of boiler 1 exhaust gasses temperature on the specific CO_2 emissions and sustainability index.

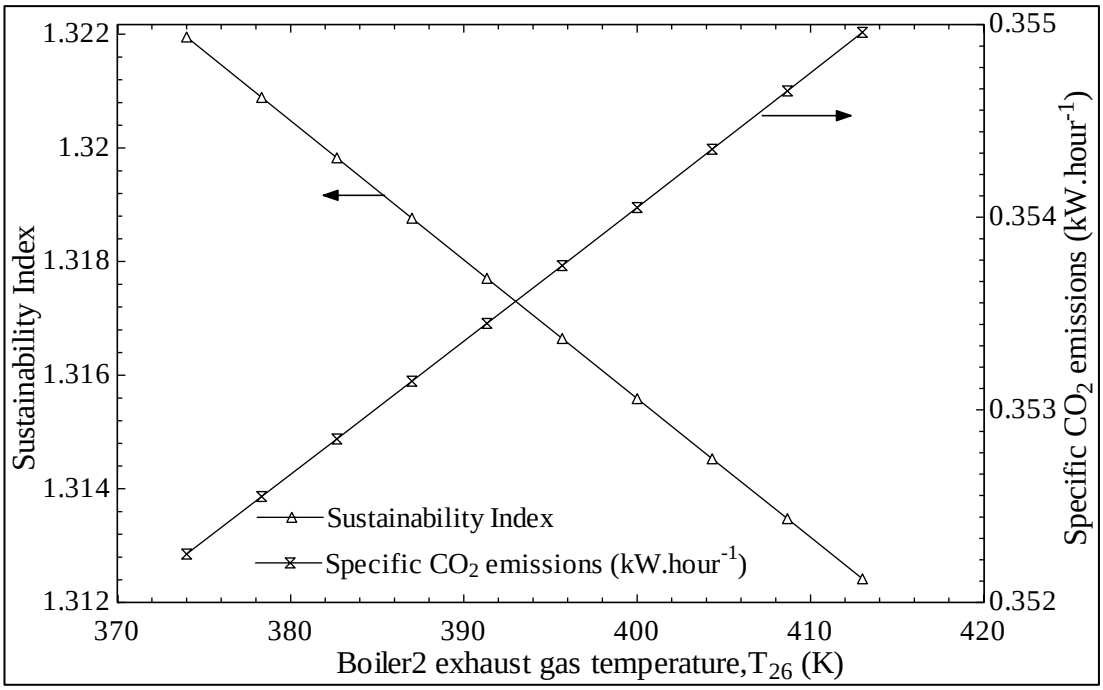

Figure 5.21: Effect of boiler 2 exhaust gasses temperature on the specific CO_2 emissions and sustainability index.

5.4 Validation of the Results

In order to validate the results, the multi-generation system was scaled down to match the system with published paper previously (Ahmadi P. D., 2013), (Dincer I, Rosen MA, 2013). Obtained results are compared in Table 6.

Table 6: Evaluation of the current thesis results with the previous simulations done by other researcher

Parameter (Unit)	Current study	Published study: (Ahmadi, 2013)	Published Study: (Dincer I, Rosen MA, 2013)
Biomass flow rate, $\dot{m}_{biomass}$ ($kg.s^{-1}$)	0.125	0.3	0.3
Heating load, $\dot{Q}_{heating}$ (kW)	1332	2383	2617
Cooling load, $\dot{Q}_{Cooling}$ (kW)	223.8	2560	610.7
Electricity, $\dot{W}_{net}$ (kW)	372.8	500.47	671
Overall utilization factor	2.096	1.971	1.684
Exergy efficiency, ψ_{MG} (%)	24.03	28.82	22.20
COP_{en} of SEACS (-)	0.8177	1.63 (DEACS)	0.44
H_2 production mass flow rate, $\dot{m}_{Hydrogen}$ (kg/day)	3.9408	2	3.14
Specific CO_2 emission, ε_{MG} (kg/MWh)	353.8	358	518.8
Sustainability Index	1.316	1.408	1.28
Power to heating ratio (-)	0.3522	0.19	0.26
Power to cooling ratio (-)	2.091	0.2	1.09

Chapter 6

CONCLUSION

In the current study, a multi-generation cycle was designed to include: (a) a single effect absorption cooling system (SEACS), working with LiBr/Water solution, (b) an organic Rankine cycle (ORC) working with n-heptane, (c) an air conditioning system based on dehumidification (AC), (d) a combustion chamber (CC), and (e) an electrolyzer. This system is modeled to produce electricity, heating, cooling, hydrogen and dry air.

Calculating the amount of output depends on the inlet fuel (pine sawdust as a biofuel). By consumption of 0.123 kg/s of biofuel the energetic and exergetic efficiency were conducted 2.096 and 24.03%, respectively. The CO_2 emission is 0.2001 kg/s, which represents sustainability index by 1.316 and specific CO_2 emission by 353.8 kg/MWh.

Further, the comprehensive parametric study was done to investigate the effect of varying important parameter, such as ambient temperature, ORC boiler outlet temperature, RSRC boiler outlet temperature, biofuel mass flow rate, and injected heat to the generator.

As expected, it showed an increase in the biofuel mass flow rate (from 0.123 kg/s to 0.22 kg/s); was resulted in an increased in the amount of productions of the cycles.

Moreover, it causes an upward trend for total exergy destruction (from 1464 kW to 2004 kW) and exergy efficiency (from 23.61% to 35.14%), and downward trend for overall utilization factor (from 2.11 to 1.731). Furthermore, by increasing the exergy performance, sustainability index of the plant improved from 1.309 to 1.542. Since overall utilization factor declined, and more CO_2 is emitted, the specific CO_2 emission rose from 351.5 kg/MWh to 428.5 kg/MWh.

An increase in the sink temperature (from 281 K to 337 K), results in an increase for total exergy destruction (from 1439 kW to 1602 kW) and exergy efficiency (from 26.21% to 16.08%). By decreasing the exergy performance, sustainability index declined from 1.355 to 1.192.

In addition, an increase in the outlet temperature of the RSRC boiler (from 1010 K to 1245 K), results in an increase for total exergy destruction (from 1472 kW to 1518 kW), and a decrease in exergy efficiency (from 24.28 % to 19.69 %) and energy efficiency (from 2.101 to 2.011). By reducing the exergy performance, sustainability index of the plant declined from 1.321 to 1.245. Since overall utilization factor declined, specific CO_2 emission rose from 352.3 kg/MWh to 355 kg/MWh.

An increase in the ORC boiler output temperature (from 374 K to 413 K), result in an increase for total exergy destruction (from 1467 kW to 1480 kW), and decrease in exergy efficiency (from 24.35 % to 23.80 %) and overall utilization factor (from 2.106 to 2.09). By decreasing the exergy performance, sustainability index of the plant declined from 1.32 to 1.312. Since overall utilization factor declined, therefore CO_2 emission rose from 353 kg/MWh to 368.9 kg/MWh.

As a general interpretation on performed parametric study, increase in boilers outlet temperature and sink temperature have a negative effect on the environmental factors of the system. Moreover, parametric study illustrates that for an increase in biofuel mass flow rate sustainability of the system increased, but it has negative effect on environmental factors, due to the rise in specific CO_2 emissions.

REFERENCES

Dincer, I., & Gadalla, M. (2012). Performance analysis of a novel integrated geothermal-based system for multi-generation applications. *Applied Thermal Engineering* .

Ahmadi, P. (2011). Greenhouse gas emission and exergo-environmental analyses of a trigeneration energy system. *International Journal of Greenhouse Gas Control*.

Ahmadi, P. (2012). Exergo-environmental analysis of an integrated organic Rankine cycle for trigeneration. *Energy Conversion and Management* .

Ahmadi, P., & D. I. (2012). Exergo-environmental analysis of an integrated organic Rankine cycle for trigeneration. *Energy Conversion and Management*.

Ahmadi, P. (2012). Multi-objective exergy-based optimization of a polygeneration energy system using an evolutionary algorithm. *Energy*.

Ahmadi, P. (2013). Modeling, analysis and optimization of integrated energy systems for multigeneration purposes. *Faculty of Engineering and Applied Science*.

Ameri, M. (2013). Enhancing the efficiency of crude oil transportation pipeline: a novel approach. *International Journal of Exergy*.

AV, A. (2008). An analysis of SOFC/GT CHP system based on exergetic performance criteria . *International Journal of Hydrogen Energy* .

Basu, K. (2006). Combustion and gasification in fluidized beds. *CRC press*.

Bingöl, T. (2011). Exergy based performance analysis of high efficiency poly-generation systems for sustainable building applications. *Energy and Buildings*.

Buck, M. (2007). Solar-assisted small solar tower trigeneration systems. *Transactions-American Society Of Mechanical Engineers Journal Of Solar Energy Engineering*.

Calva, K. (2005). Thermal integration of trigeneration systems. *Applied Thermal Engineering*.

Chum, H. L. (2001). Biomass and renewable fuels . *Fuel Processing Technology*.

Cohce, L. (2011). Energy and exergy analyses of a biomass-based hydrogen production system. *Bioresource Technology*.

Dincer. (2012). Exergy. *Energy, environment and sustainable development.*

Dincer I, Rosen MA. (2013). Development and assessment of an integrated biomass-based multi-generation energy system. *Energy* .

Dincer, I. (2012). Renewable-energy-based multigeneration systems. *International Journal of Energy Research*.

Dong, L. (2009). Development of small-scale and micro-scale biomass-fuelled CHP systems. *Applied Thermal Engineering*.

Ehyaei, J. (2015). Optimization of fog inlet air cooling system for combined cycle power plants using genetic algorithm. *Applied Thermal Engineering*.

FA, S. (2010). Energy analysis of a trigeneration plant based on solid oxide fuel cell and organic Rankine cycle. *International Journal of Hydrogen Energy* .

Ferreira, S. (2001). Comparison of externally fired and internal combustion gas turbines using biomass fuel. *ASME J. Energy Resourc. Technol*.

Franco, G. (2005). Perspectives for the use of biomass as fuel in combined cycle power plants. *International Journal of Thermal Sciences*.

Ganjehkaviri, U. (2014). Energy analysis and multi-objective optimization of an internal combustion engine-based CHP system for heat recovery. *Entropy*.

H.L., & Chum, R. (2001). Overend, biomass and renewable fuels. *Fuel Process*.

Hosseini, A. (2011). Thermodynamic modelling of an integrated solid oxide fuel cell and micro gas turbine system for desalination purposes . *International Journal of Energy Research*.

J, M. (2004). Feasibility of a new domestic CHP trigeneration with heat pump. *Applied Thermal Engineering*.

J, P. (2004). Feasibility of a new domestic CHP trigeneration with heat pump availability analysis. *Applied Thermal Engineering*.

Kay. (1938). Liquid-vapor phase equilibrium relations in the ethane-n-heptane system. *Industrial & Engineering Chemistry*.

Khaliq, A. (2009). Exergy analysis of gas turbine trigeneration system for combined production of power heat and refrigeration. *International Journal of Refrigeration*.

Lian. (2010). A thermoeconomic analysis of biomass energy for trigeneration. *Applied Energy* .

MA, R. (2003). Exergoeconomic analysis of power plants operating on various fuels. *Applied Thermal Engineering*.

Mago, P. (2010). Analysis and optimization of the use of CHP–ORC systems for small commercial buildings. *Energy and Buildings*.

Moya, Q. (2011). Performance analysis of a trigeneration system based on a micro gas turbine and an air-cooled, indirect fired, ammonia–water absorption chiller. *Applied Energy* .

Mujeebu, S. (2009). Feasibility study of cogeneration in a plywood industry with power export to grid . *Applied Energy* .

Nami, J. (2016). Utilization of waste heat from GTMHR for hydrogen generation via combination of organic Rankine cycles and PEM electrolysis. *Energy Conversion and Management*.

Onovwiona, H. I. (2006). Residential cogeneration systems: review of the current technology. *Renewable and Sustainable Energy Reviews*.

Ozturk. (2012). Thermodynamic analysis of a solar-based multi-generation system with hydrogen production. *Applied Thermal Engineering*.

Pospisil. (2006). Comparison of cogeneration and trigeneration technology for energy supply of tertiary buildings. *WSEAS Transactions on Heat and Mass Transfer* .

Ratlamwala, T. (2010). Performance analysis of a novel integrated geothermal-based system for multi-generation applications. *Applied Thermal Engineering*.

Ratlamwala, T. (2011). Performance assessment of an integrated PV/T and triple effect cooling system for hydrogen and cooling production. *International Journal of Hydrogen Energy* .

Ratlamwala, T. (2012). Performance analysis of a novel integrated geothermal-based system for multi-generation applications. *Applied Thermal Engineering*.

RS, E. (2011). Energy and exergy analyses of a combined molten carbonate fuel cell–Gas turbine system. . *International Journal of Hydrogen Energy* .

Smith, A. (2013). Benefits of thermal energy storage option combined with CHP system for different commercial building types. *Sustainable Energy Technologies and Assessments*.

Szargut, N. (2007). Wydawnictwo Politechniki Śląskiej. *Egzergia poradnik obliczania stosowania*.

Velumani, I. (2010). Proposal of a hybrid CHP system: SOFC/microturbine/absorption chiller. *International Journal of Energy Research* .

Ziher, Q. (2006). Economics of a trigeneration system in a hospital . *Applied Thermal Engineering*.

APPENDIX

"MGS"

"surrounding states for air"

t[0]=20+273.15

h[0]=Enthalpy(Air,T=T[0])

s[0]=Entropy(Air,T=T[0],P=P[0])

p[0]=100

ex[0]=((h[0]-h[0])-t[0]*(s[0]-s[0]))

"biomass"

"C5H8O3+0.71612H2O+5.5O2+20.6905N2=5CO2+4.716H2O+20.6905N2"

MN2=MolarMass(Nitrogen)

b=0.09605221522

a=0.248769352

c=0.6551784328

m_dot[24]=m_dot[23]+m_dot[20]

p[24]=100

t[24]=1800+273.15

h[24]=Enthalpy(water,T=T[24],P=P[24])*(b)+Enthalpy(CarbonDioxide,T=T[24],P=P[24])*(a)+Enthalpy(Nitrogen,T=T[24],P=P[24])*(c)

s[24]=Entropy(water,T=T[24],P=P[24])*(b)+Entropy(CarbonDioxide,T=T[24],P=P[24])*(a)+Entropy(Nitrogen,T=T[24],P=P[24])*(c)

ex[24]=((h[24]-h[0])-t[0]*(s[24]-s[0]))

lhvdry=(400000+100600*8-0.6*(117600+100600*8))/(12+8+16*3)

lhvmoisture=(1-0.1-0.063)*lhvdry-2500*0.1

pppppp=MolarMass(CarbonDioxide)

m_dot[25]=m_dot[24]

p[25]=100

t[25]=750+273.15

t[63]=t[25]

h[25]=Enthalpy(water,T=T[25],P=P[25])*(b)+Enthalpy(CarbonDioxide,T=T[25],P=P[25])*(a)+Enthalpy(Nitrogen,T=T[25],P=P[25])*(c)

s[25]=Entropy(water,T=T[25],P=P[25])*(b)+Entropy(CarbonDioxide,T=T[25],P=P[25])*(a)+Entropy(Nitrogen,T=T[25],P=P[25])*(c)

ex[25]=((h[25]-h[0])-t[0]*(s[25]-s[0]))

m_dot[26]=m_dot[24]

p[26]=100

t[26]=397

t[26]=t[64]

h[26]=Enthalpy(water,T=T[26],P=P[26])*(b)+Enthalpy(CarbonDioxide,T=T[26],P=P[26])*(a)+Enthalpy(Nitrogen,T=T[26],P=P[26])*(c)

s[26]=Entropy(water,T=T[26],P=P[26])*(b)+Entropy(CarbonDioxide,T=T[26],P=P[26])*(a)+Entropy(Nitrogen,T=T[26],P=P[26])*(c)

ex[26]=((h[26]-h[0])-t[0]*(s[26]-s[0]))

exchemexhoustgas=(19480/44.01)*a+(9500/18.016)*b+(720/28.01)*c

m_dotconsumptionO2=m_dot[23]*5.4336*d

m_dotCO2=a*(m_dot[23]+m_dot[23]*5.43358)

ex_dotdesCC=m_dot[23]*ex[23]+m_dot[20]*ex[20]-(m_dot[24]*(ex[24]+exchemexhoustgas))

{5.5O2+20.6905N2}

d=0.2537963

e=0.7462037

airfuelratio=5.43358

m_dot[20]=5.43358*m_dot[23]

p[20]=p[0]

t[20]=25+273.15

h[20]=Enthalpy(Oxygen,T=T[20],P=P[20])*d+Enthalpy(Nitrogen,T=T[20],P=P[20])*e

s[20]=Entropy(Oxygen,T=T[20],P=P[20])*d+Entropy(Nitrogen,T=T[20],P=P[20])*e

ex[20]=((h[20]-h[0])-t[0]*(s[20]-s[0]))

m_dot[23]=0.125

p[23]=p[0]

t[23]=25+273.15

h[23]=-9442

s[23]=1.38

ex[23]=18756

m_dot[41]=0.36

p[41]=12500

h[41]=Enthalpy(Water,T=T[41],P=P[41])

s[41]=Entropy(Water,T=T[41],P=P[41])

ex[41]=((h[41]-h[0])-t[0]*(s[41]-s[0]))

m_dot[42]=m_dot[41]

p[42]=3900

t[42]=400+273.15

x[42]=0

h[42]=Enthalpy(Water,T=T[42],P=P[42])

s[42]=Entropy(Water,T=T[42],P=P[42])

ex[42]=((h[42]-h[0])-t[0]*(s[42]-s[0]))

m_dot[43]=m_dot[41]

p[43]=p[42]

t[43]=t[41]

h[43]=Enthalpy(Water,t=t[43],P=P[43])

s[43]=Entropy(Water,t=t[43],P=P[43])

ex[43]=((h[43]-h[0])-t[0]*(s[43]-s[0]))

m_dot[44]=m_dot[41]

p[44]=20

t[44]=75+273.15

h[44]=Enthalpy(Water,T=T[44],P=P[44])

s[44]=Entropy(Water,T=T[44],P=P[44])

ex[44]=(h[44]-h[0])-t[0]*(s[44]-s[0])

m_dot[38]=m_dot[41]

p[38]=p[44]

x[38]=0

t[38]=Temperature(Water,P=P[38],x=x[38])

h[38]=Enthalpy(Water,x=x[38],P=P[38])

s[38]=Entropy(Water,x=x[38],P=P[38])

ex[38]=((h[38]-h[0])-t[0]*(s[38]-s[0]))

v[38]=Volume(Water,x=x[38],P=P[38])

m_dot[37]=m_dot[41]

p[37]=p[41]

t[37]=t[38]

h[37]=Enthalpy(Water,T=T[37],P=P[37])

s[37]=Entropy(Water,T=T[37],P=P[37])

ex[37]=((h[37]-h[0])-t[0]*(s[37]-s[0]))

m_dot[36]=m_dot[41]

p[36]=p[41]

t[36]=Temperature(Water,P=P[36],h=h[36])

{h[36]=Enthalpy(Water;T=T[36];P=P[36])}

s[36]=Entropy(Water,T=T[36],P=P[36])

ex[36]=((h[36]-h[0])-t[0]*(s[36]-s[0]))

m_dot[22]=m_dot[41]

p[22]=20

x[22]=1

t[22]=Temperature(Water,P=P[22],x=x[22])

h[22]=Enthalpy(Water,x=x[22],P=P[22])

s[22]=Entropy(Water,T=T[22],P=P[22])

ex[22]=(h[22]-h[0])-t[0]*(s[22]-s[0])

m_dot[21]=m_dot[41]

p[21]=p[41]

h[21]=Enthalpy(Water,T=T[21],P=P[21])

s[21]=Entropy(Water,T=T[21],P=p[21])

ex[21]=h[21]-h[0]-t[0]*(s[21]-s[0])

{m_dot[39]=0,5}

p[39]=p[0]

t[39]=25+273.15

h[39]=Enthalpy(Water,T=T[39],P=P[39])

s[39]=Entropy(Water,T=T[39],P=P[39])

ex[39]=((h[39]-h[0])-t[0]*(s[39]-s[0]))

m_dot[31]=m_dot[39]

p[31]=p[39]

t[31]=t[38]

h[31]=Enthalpy(Water,t=t[31],P=P[31])

s[31]=Entropy(Water,t=t[31],P=P[31])

ex[31]=((h[31]-h[0])-t[0]*(s[31]-s[0]))

(m_dot[22]*h[22]-m_dot[38]*h[38])=m_dot[31]*h[31]-m_dot[39]*h[39]
"""Cond1"""

Wheating1=m_dot[31]*h[31]-m_dot[39]*h[39]

ex_Wheating1=(1-t[0]/tCond1)*Wheating1

m_dot[22]*ex[22]+m_dot[39]*ex[39]=ex_dotdesCon1+m_dot[31]*ex[31]+m_dot[38]*ex[38]

(m_dot[44]*h[44]-m_dot[22]*h[22])*0.8=Q_dot_HX2

m_dot[21]*h[21]-m_dot[37]*h[37]=(m_dot[44]*h[44]-m_dot[22]*h[22])*0.8

m_dot[44]*ex[44]+m_dot[37]*ex[37]=m_dot[21]*ex[21]+m_dot[22]*ex[22]+ex_dotdesHX2

w_dotHPST=m_dot[41]*(h[41]-h[42])

ex_dotdesHPST+m_dot[42]*ex[42]+w_dotHPST=m_dot[41]*ex[41]

w_dotLPST=m_dot[43]*(h[43]-h[44])

ex_dotdesLPST+m_dot[44]*ex[44]+w_dotLPST=m_dot[43]*ex[43]

w_dotP2=m_dot[38]*(v[38]*(p[37]-p[38]))

w_dotP2+m_dot[38]*ex[38]=m_dot[37]*ex[37]+ex_dotdesP2

m_dot[35]=0.63

p[35]=1000

t[35]=Temperature(n-Heptane,P=P[35],h=h[35])

"h[35]=Enthalpy(n-Heptane;T=T[35];P=P[35])"

s[35]=Entropy(n-Heptane,T=T[35],P=P[35])

ex[35]=((h[35]-h[0])-t[0]*(s[35]-s[0]))

m_dot[34]=m_dot[35]

p[34]=200

t[34]=305+273.15

h[34]=Enthalpy(n-Heptane,T=T[34],P=P[34])

s[34]=Entropy(n-Heptane,T=T[34],P=P[34])

ex[34]=((h[34]-h[0])-t[0]*(s[34]-s[0]))

w_dotT=m_dot[35]*(h[35]-h[34])

ex_dotdesT+m_dot[34]*ex[34]+w_dotT=m_dot[35]*ex[35]

m_dot[33]=m_dot[35]

p[33]=p[34]

x[33]=0

t[33]=Temperature(n-Heptane,P=P[33],x=x[33])

h[33]=Enthalpy(n-Heptane,x=x[33],P=P[33])

s[33]=Entropy(n-Heptane,x=x[33],P=P[33])

ex[33]=((h[33]-h[0])-t[0]*(s[33]-s[0]))

0.8*(m_dot[34]*h[34]-m_dot[33]*h[33])=m_dot[36]*h[36]-m_dot[21]*h[21]

m_dot[34]*ex[34]+m_dot[21]*ex[21]=m_dot[33]*ex[33]+m_dot[36]*ex[36]+ex_dotdesHX1

m_dot[32]=m_dot[35]

p[32]=p[35]

t[32]=t[33]

h[32]=Enthalpy(n-Heptane,T=T[32],P=P[32])

s[32]=Entropy(n-Heptane,T=T[32],P=P[32])

ex[32]=((h[32]-h[0])-t[0]*(s[32]-s[0]))

v[32]=Volume(n-Nonane,T=T[32],P=P[32])

w_dotP1=m_dot[33]*(v[32]*(p[32]-p[33]))

m_dot[33]*ex[33]+w_dotP1=m_dot[32]*ex[32]+ex_dotdesP1

m_dot[24]*ex[24]+m_dot[42]*ex[42]+m_dot[36]*ex[36]=m_dot[41]*ex[41]+m_dot[25]*ex[25]+m_dot[43]*ex[43]+ex_dotdesB1

0.8*(m_dot[24]*h[24]-m_dot[25]*h[25])=m_dot[41]*h[41]+m_dot[43]*h[43]-(m_dot[42]*h[42]+m_dot[36]*h[36])

m_dot[25]*ex[25]+m_dot[32]*ex[32]=m_dot[35]*ex[35]+m_dot[26]*ex[26]+ex_dotdesB2

0.8*m_dot[24]*(h[25]-h[26])=m_dot[35]*(h[35]-h[32])

m_dot[27]=m_dot[24]

p[27]=p[24]

t[27]=t[0]+5

h[27]=Enthalpy(water,T=T[27],P=P[27])*(b)+Enthalpy(CarbonDioxide,T=T[27],P=P[27])*(a)+Enthalpy(Nitrogen,T=T[27],P=P[27])*(c)

s[27]=Entropy(water,T=T[27],P=P[27])*(b)+Entropy(CarbonDioxide,T=T[27],P=P[27])*(a)+Entropy(Nitrogen,T=T[27],P=P[27])*(c)

ex[27]=((h[27]-h[0])-t[0]*(s[27]-s[0]))

m_dot[1]=1.145

x[1]=0.5225

p[1]=1

t[1]=32+273.15

s[1]=s_LiBrH2O(T[1],x[1])

h[1]=h_LiBrH2O(T[1],x[1])

ex[1]=((h[1]-h[0])-t[0]*(s[1]-s[0]))

v[1]=1/rho_LiBrH2O(T[1],X[1])

m_dot[2]=m_dot[1]

x[2]=x[1]

p[2]=4.81

t[2]=t[1]

s[2]=s_LiBrH2O(T[2],x[2])

h[2]=h_LiBrH2O(T[2],x[2])

ex[2]=((h[2]-h[0])-t[0]*(s[2]-s[0]))

w_dotp3=m_dot[2]*v[1]*(p[2]-p[1])

w_dotp3+m_dot[1]*ex[1]=m_dot[2]*ex[2]+ex_dotdesp3

m_dot[3]=m_dot[1]

x[3]=x[1]

t[3]=57.9+273.15

p[3]=p[2]

{h[3]=h_LiBrH2O(t[3];x[3])}

s[3]=s_LiBrH2O(t[3],x[3])

ex[3]=((h[3]-h[0])-t[0]*(s[3]-s[0]))

m_dot[4]*x[4]=m_dot[3]*x[3]

x[4]=0.5694

t[4]=69.8+273.15

p[4]=p[2]

h[4]=h_LiBrH2O(T[4],x[4])

s[4]=s_LiBrH2O(t[4],x[4])

ex[4]=((h[4]-h[0])-t[0]*(s[4]-s[0]))

m_dot[5]=m_dot[4]

x[5]=x[4]

p[5]=p[2]

t[5]=32.2+273.15

h[5]=h_LiBrH2O(T[5],x[5])

s[5]=s_LiBrH2O(T[5],x[5])

ex[5]=((h[5]-h[0])-t[0]*(s[5]-s[0]))

(m_dot[4]*h[4]-m_dot[5]*h[5])*0.8=(m_dot[3]*h[3]-m_dot[2]*h[2])

m_dot[4]*ex[4]-m_dot[5]*ex[5]=m_dot[3]*ex[3]-m_dot[2]*ex[2]+ex_dotdesHX3

m_dot[6]=m_dot[4]

x[6]=x[4]

t[6]=32.2+273.15

p[6]=p[1]

h[6]=h_LiBrH2O(T[6],x[6])

s[6]=s_LiBrH2O(t[6],x[6])

ex[6]=((h[6]-h[0])-t[0]*(s[6]-s[0]))

m_dot[7]=m_dot[3]-m_dot[4]

p[7]=p[2]

t[7]=67+273.15

h[7]=Enthalpy(Water,T=T[7],P=P[7])

s[7]=Entropy(Water,T=T[7],P=P[7])

ex[7]=((h[7]-h[0])-t[0]*(s[7]-s[0]))

m_dot[8]=m_dot[7]

p[8]=p[7]

t[8]=32.19+273.15

h[8]=Enthalpy(Water,T=T[8],P=P[8])

s[8]=Entropy(Water,T=T[8],P=P[8])

ex[8]=((h[8]-h[0])-t[0]*(s[8]-s[0]))

m_dot[9]=m_dot[7]

p[9]=p[1]

x[9]=Quality(Water,T=T[9],h=h[9])

t[9]=7+273.15

h[9]=h[8]

s[9]=Entropy(Water,x=x[9],t=t[9])

ex[9]=((h[9]-h[0])-t[0]*(s[9]-s[0]))

m_dot[10]=m_dot[7]

p[10]=p[9]

x[10]=1

t[10]=7+273.15

h[10]=Enthalpy(Water,x=x[10],P=P[10])

s[10]=Entropy(Water,p=p[10],t=t[10])

ex[10]=((h[10]-h[0])-t[0]*(s[10]-s[0]))

{m_dot[18]}

p[18]=100

t[18]=t[0]

h[18]=Enthalpy(Water,t=t[18],P=P[18])

s[18]=Entropy(Water,t=t[18],P=P[18])

ex[18]=((h[18]-h[0])-t[0]*(s[18]-s[0]))

m_dot[19]=m_dot[18]

p[19]=100

t[19]=t[1]

h[19]=Enthalpy(Water,T=T[19],P=P[19])

s[19]=Entropy(Water,T=T[19],P=P[19])

ex[19]=((h[19]-h[0])-t[0]*(s[19]-s[0]))

{m_dot[11]}

p[11]=100

t[11]=t[0]+10

h[11]=Enthalpy(air,T=T[11])

s[11]=Entropy(air,T=T[11],P=P[11])

ex[11]=((h[11]-h[0])-t[0]*(s[11]-s[0]))

m_dot[12]=m_dot[11]

t[12]=t[9]+6

p[12]=p[11]

h[12]=Enthalpy(Air,T=T[12])

s[12]=Entropy(air,T=T[12],P=P[12])

ex[12]=((h[12]-h[0])-t[0]*(s[12]-s[0]))

(m_dot[26]*h[26]-m_dot[27]*h[27])=q_dotGg

q_dotG+m_dot[3]*h[3]=m_dot[4]*h[4]+m_dot[7]*h[7]

ex_dotG=((tG-t[0])/tG)*q_dotG

tG=(t[4]+t[3])/2

ex[3]*m_dot[3]+ex_dotG=ex[4]*m_dot[4]+ex[7]*m_dot[7]-Des_dotG

q_dotCond1=m_dot[7]*h[7]-m_dot[8]*h[8]

ex_dotCond1=((tCond1-t[0])/tCond1)*q_dotCond1

tCond1=(t[8]+t[7])/2

ex_dotCond1+m_dot[7]*ex[7]=Des_dotCond1+m_dot[8]*ex[8]

COP=q_dotEva/q_dotG

copp=ex_dotevaporator/ex_dotG

q_dotEva=m_dot[10]*(h[10]-h[9])

ex_dotevaporator=((t[0]-tEva)/tEva)*q_dotEva

(t[9]+t[10])/2=tEva

q_dotEva=m_dot[11]*h[11]-m_dot[12]*h[12]

Des_dotEva+m_dot[10]*ex[10]+m_dot[12]*ex[12]=m_dot[11]*ex[11]+m_dot[9]*ex[9]

coolingload=m_dot[12]*(h[11]-h[12])-q_dotoutdryer

ex_dotcoolingload=coolingload*(1-t[0]/t[11])

q_dotAbs=m_dot[19]*h[19]-m_dot[18]*h[18]

q_dotAbs=m_dot[10]*h[10]+m_dot[6]*h[6]-m_dot[1]*h[1]

ex_dotAbs=((tAbs-t[0])/tAbs)*q_dotAbs

tAbs=(t[1]+t[6])/2

m_dot[10]*ex[10]+m_dot[6]*ex[6]+m_dot[18]*ex[18]=Des_dotabs+m_dot[1]*ex[1]+m_dot[19]*ex[19]

Wheating2=q_dotAbs

exWheating2=(1-t[0]/tAbs)*Wheating2

"for electrolyzer"

(m_dot[29]*exchemH2O)+m_dot[29]*ex[29]+etaelectrolyzer*w_dotT=m_dot[28]*exchemH2+m_dot[28]*ex[28]+m_dot[30]*ex[30]+m_dot[30]*exchemO2+ex_dotdesElectrolyzer

etaelectrolyzer=0.56

W_lossElectrolyzer=(1-etaelectrolyzer)*w_dotT

HHV=141800

MH2=MolarMass(H2)

```
m_dot[28]=(etaelectrolyzer*w_dotT*1)/HHV

 p[28]=100

t[28]=60+273.15

h[28]=Enthalpy(H2,T=T[28])

s[28]=Entropy(H2,T=T[28],P=P[28])

ex[28]=((h[28]-h[0])-t[0]*(s[28]-s[0]))

exchemH2=(236.09*1000)/MH2

exchemH2*m_dot[28]=ex_doth2

MO2=MolarMass(O2)

m_dot[30]=(m_dot[28]/MH2)*(0.5)*MO2

p[30]=100

t[30]=60+273.15

h[30]=Enthalpy(O2,T=T[30])

s[30]=Entropy(O2,T=T[30],P=P[30])

ex[30]=((h[30]-h[0])-t[0]*(s[30]-s[0]))

exchemO2=(3.97*1000)/MO2

MH2O=MolarMass(Water)

m_dot[29]=(m_dot[28]/MH2)*MH2O

t[29]=25+273.15
```

p[29]=100

h[29]=Enthalpy(Water,T=T[29],P=p[29])

s[29]=Entropy(Water,T=T[29],P=P[29])

ex[29]=((h[29]-h[0])-t[0]*(s[29]-s[0]))

exchemH2O=(0.9*1000)/MH2O

m_dotwater=m_dot[29]*3.600

m_dotH2=m_dot[28]*3600

{m_dot[13]}

t[13]=t[12]

p[13]=p[12]

h[13]=Enthalpy(Air,T=T[13])

s[13]=Entropy(air,T=T[13],P=P[13])

ex[13]=((h[13]-h[0])-t[0]*(s[13]-s[0]))

m_dot[40]=m_dot[12]-m_dot[13]

t[40]=t[12]

p[40]=p[12]

h[40]=Enthalpy(Air,T=T[40])

s[40]=Entropy(air,T=T[40],P=P[40])

ex[40]=((h[40]-h[0])-t[0]*(s[40]-s[0]))

```
m_dot[16]=m_dot[13]

t[16]=t[0]

p[16]=p[13]

h[16]=Enthalpy(Air,T=T[16])

s[16]=Entropy(air,T=T[16],P=P[16])

ex[16]=((h[16]-h[0])-t[0]*(s[16]-s[0]))

m_dot[14]=0.1

t[14]=t[0]

p[14]=p[0]

rh[14]=0.8

h[14]=Enthalpy(AirH2O,T=T[14],r=rh[14],P=P[14])

s[14]=Entropy(AirH2O,T=T[14],r=rh[14],P=P[14])

ex[14]=((h[14]-h[0])-t[0]*(s[14]-s[0]))

omega[14]=HumRat(AirH2O,T=T[14],r=rh[14],P=P[14])

m_dot[15]=m_dot[14]

t[15]=t[0]-4

p[15]=p[0]

rh[15]=1

h[15]=Enthalpy(AirH2O,T=T[15],r=rh[15],P=P[15])
```

s[15]=Entropy(AirH2O,T=T[15],r=rh[15],P=P[15])

ex[15]=((h[15]-h[0])-t[0]*(s[15]-s[0]))

omega[15]=HumRat(AirH2O,T=T[15],r=rh[15],P=P[15])

p[17]=p[14]

t[17]=t[15]

h[17]=Enthalpy(Water,T=T[17],P=P[17])

s[17]=Entropy(Water,T=T[17],P=P[17])

ex[17]=((h[17]-h[0])-t[0]*(s[17]-s[0]))

q_dotoutdryer=m_dot[16]*h[16]-m_dot[13]*h[13]

ex_dotq_dotoutdryer=q_dotoutdryer*(1-t[0]/t[15])

m_dot[14]*omega[14]=m_dot[15]*omega[15]+m_dot[17]

m_dot[14]*h[14]=q_dotoutdryer+m_dot[15]*h[15]+m_dot[17]*h[17]

ex_dotdesDryer=m_dot[13]*ex[13]-ex_dotq_dotoutdryer-m_dot[16]*ex[16]

w_dotHPST+w_dotLPST-(w_dotP2+w_dotP1)=electricity

DWH=Wheating2+Wheating1

ex_dot_PUMPS=ex_dotdesP1+ex_dotdesP3+ex_dotdesP2

EFF=(coolingload+q_dotCond1+DWH+electricity+m_dot[28]*HHV+m_dot[15]*h[15])/((lhvmoisture*m_dot[23]))

pp=t[26]-t[27]

electricity/(DWH+q_dotCond1)=PW

electricity/(q_dotEva)=PC

effex=((ex_Wheating1+exWheating2+ex_dotcoolingload+ex_dotCond1+ex_doth2+electricity+m_dot[15]*ex[15])/((m_dot[23]*ex[23])))

ex_destotal=ex_dotdesElectrolyzer+ex_dotdesB2+ex_dotdesB1+ex_dotdesP1+ex_dotdesHX1+ex_dotdesP2+ex_dotdesT+ex_dotdesLPST+ex_dotdesHPST+ex_dotdesCon1+ex_dotdesCC+ex_dotdesHX2

3600*m_dotCO2/(coolingload+q_dotCond1+DWH+electricity+m_dot[28]*HHV+m_dot[15]*h[15])=co_norm

SI=1/(1-effex)